भारतीय मानक
Indian Standard

IS 18902 : 2024
ISO/TR 19057 : 2017

नैनो प्रौद्योगिकी — नैनो सामग्री की जैव स्थायित्वता का आकलन करने के लिए अकोशिकीय इन-विट्रो परीक्षणों और पद्धतियों का उपयोग और अनुप्रयोग

Nanotechnologies — Use and Application of Acellular In-vitro Tests and Methodologies to Assess Nanomaterial Biodurability

ICS 07.120

भारतीय मानक ब्यूरो
BUREAU OF INDIAN STANDARDS
मानक भवन, 9 बहादुर शाह ज़फर मार्ग, नई दिल्ली - 110002
MANAK BHAVAN, 9 BAHADUR SHAH ZAFAR MARG
NEW DELHI - 110002
www.bis.gov.in   www.standardsbis.in

September 2024

Price Group 14

Medical Biotechnology and Medical Nanotechnology Sectional Committee, MHD 20

NATIONAL FOREWORD

This Indian Standard which is identical to ISO 19057 : 2017 'Nanotechnologies — Use and application of acellular in vitro tests and methodologies to assess nanomaterial biodurability' issued by the International Organization for Standardization was adopted by Bureau of Indian Standards on the recommendation of the 'Medical Biotechnology and Medical Nanotechnology Sectional Committee' and approval of the Medical Equipment and Hospital Planning Division Council.

The text of ISO standard has been approved as suitable for publication as an Indian Standard without deviations. Certain conventions are, however, not identical to those used in Indian Standard. Attention is particularly drawn to the following:

a) Wherever the words 'International Standard' appear referring to this standard, they should be read as 'Indian Standard'; and

b) Comma (,) has been used as a decimal marker while in Indian Standards, the current practice is to use a point (.) as the decimal marker.

In reporting the result of a test or analysis made in accordance with this standard, if the final value, observed or calculated, expressing the result of a test or analysis, shall be rounded off in accordance with IS 2 : 2022 'Rules for rounding off numerical values (*second revision*)'.

Contents

Indian Standard

NANOTECHNOLOGIES — USE AND APPLICATION OF ACELLULAR IN-VITRO TESTS AND METHODOLOGIES TO ASSESS NANOMATERIAL BIODURABILITY

1 Scope

This document reviews the use and application of acellular *in vitro* tests and methodologies implemented in the assessment of the biodurability of nanomaterials and their ligands in simulated biological and environmental media.

This document is intended to focus more on acellular *in vitro* methodologies implemented to assess biodurability and, therefore, excludes the general review of relevant literature on *in vitro* cellular or animal biodurability tests.

2 Normative references

There are no normative references in this document.

3 Terms and definitions

For the purposes of this document, the following terms and definitions apply.

ISO and IEC maintain terminological databases for use in standardization at the following addresses:

— IEC Electropedia: available at http://www.electropedia.org/

— ISO Online browsing platform: available at http://www.iso.org/obp

3.1
bioaccumulation
process of accumulation of a substance in organisms or parts

[SOURCE: ISO/TR 13329:2012, 3.3]

3.2
biodegradation
degradation due to the biological environment

Note 1 to entry: Biodegradation might be modelled by *in vitro* tests.

[SOURCE: ISO/TR 13329:2012, 3.4]

3.3
biodurability
ability of a material to resist *dissolution* (3.6) and mechanical disintegration from chemical and physical clearance mechanisms

[SOURCE: ISO/TR 13329:2012, 3.5, modified]

3.4
biopersistence
ability of a material to persist in a tissue in spite of the tissue's physiological clearance mechanisms and environmental conditions

[SOURCE: EN 18748:1999]

3.5
dispersion
microscopic multi-phase system in which discontinuities of any state (solid, liquid or gas: discontinuous phase) are dispersed in a continuous phase of a different composition or state

[SOURCE: ISO 26824:2013, 16.5]

3.6
dissolution
process of obtaining a solution containing the analyte of interest

Note 1 to entry: Dissolution is the act of dissolving and the resulting species may be molecular or ionic.S

[SOURCE: ISO 17733:2015, 3.4.10, modified]

3.7
ligands
atoms or groups joined to the central atom

[SOURCE: IUPAC Recommendations 1994]

3.8
nanomaterial
material with any external dimension in the nanoscale or having internal structure or surface structure in the nanoscale

Note 1 to entry: This generic term is inclusive of nano-object and nanostructured material.

Note 2 to entry: See also engineered nanomaterial, manufactured nanomaterial and incidental nanomaterial.

[SOURCE: ISO/TS 80004-1:2015, 2.4]

3.9
nanoparticle
nano-object with all three external dimensions in the nanoscale

Note 1 to entry: If the lengths of the longest to the shortest axes of the nano-object differ significantly (typically by more than three times), the terms nanorod or nanoplate are intended to be used instead of the term nanoparticle.

[SOURCE: ISO/TS 27687:2008, 4.1]

3.10
specific surface area for powders
absolute surface area of the sample divided by sample mass and is therefore expressed in units of m^2/g or kg

[SOURCE: ISO 9277:2010, 3.11, modified]

3.11
suspension
heterogeneous mixture of materials comprising a liquid and a finely dispersed solid material

[SOURCE: ISO/TS 80004-6:2013, 2.13]

4   Symbols and abbreviated terms

AAS   Atomic absorption spectroscopy

AF4   Asymmetrical flow field flow fractionation

AgNPs   Silver nanoparticles

ATR-FTIR	Attenuated total reflectance-Fourier transform infrared spectroscopy
AuNPs	Gold nanoparticles
$CdSe_{core}/ZnS_{shell}$	Cadmium-selenium (core) and zinc sulfide (shell)
CE	Capillary electrophoresis
CFS	Continuous flow system
CNTs	Carbon nanotubes
CPE	Cloud-point extraction
CuONPs	Copper oxide nanoparticles
Da	Dalton
DMEM	Dulbecco's Modified Eagle's Medium
DOM	Dissolved organic matter
EPA	US. Environmental Protection Agency
FFFF	Flow field flow fractionation
FTIR	Fourier transform infrared spectroscopy
GC-MS	Gas chromatography–mass spectrometry
GPC	Gel permeation chromatography
HPCIC	High-performance chelation ion chromatography
HRP	Horseradish peroxidase
ICP-MS	Inductively coupled plasma-mass spectrometry
ICP-OES	Inductively coupled plasma-optical emission spectrometry
SNMS/TOF-SIMS	Secondary neutral mass spectrometry/time-of-flight secondary ion mass spectrometry
LC-MS	Liquid chromatography-mass spectrometry
LC-MS/MS	Liquid chromatography-mass spectroscopy-mass spectroscopy
MALDI-TOF-MS	Matrix-assisted laser desorption/ionization time-of-flight mass spectrometry
m/z	Mass-to-charge ratios
MWCNTs	Multi-wall carbon nanotubes
NaCl	Sodium chloride
NP	Nanoparticle
NIOSH	U. S. National Institute for Occupational Safety and Health
NSL	Nanosphere lithography
PAP	Pulmonary alveolar proteinosis

PBPK	Physiologically-based pharmacokinetic
PSF	Phagolysosomal simulant fluid
QDs	Quantum dots
QQQ	Triple quadrupole
QTOF	Quadrupole time-of-flight
REACH	Registration, evaluation, authorisation and restriction of chemicals
RPMI	Roswell Park Memorial Institute
SDS	Sodium dodecyl sulfate
SiO_2	Silicon dioxide
SLF	Simulated lung fluid
spICP-MS	Single particle inductively coupled plasma-mass spectrometry
SPE	Solid-phase extraction
SPF	Simulated physiological fluids
SPR	Surface Plasmon Resonance
SS	Simulated saliva
SSW	Simulated sweat
SUF	Simulant ultrafiltrate fluid
SWCNTs	Single-wall carbon nanotubes
TBOs	Tungsten blue oxides
TiO_2NPs	Titanium dioxide nanoparticles
UV-Vis spectroscopy	Ultraviolet-visible spectroscopy
WO_3	Tungsten trioxide
ZnONPs	Zinc oxide nanoparticles

5   Background including need for assessing the biodurability of particles

The tendency of a given inhaled particle or fibre to cause chronic disease is strongly related to the duration of residence time in the pulmonary environment. Biopersistent particles and fibres are defined as materials that resist clearance from the body through physical and chemical means. Resistance to physical clearance may result through their resistance to phagocytosis by alveolar macrophages. Resistance to clearance by chemical and physical means, also known as biodurability, may result through their resistance to chemical dissolution. Particles and fibres that are amenable to dissolution may release components which may contribute to their adverse health effects. Similar resistance to chemical dissolution and/or biodegradation of the attached ligands in environmental media may also produce biodurable nanomaterials.

Historical experiences with micrometre-scale mineral particles and fibres provide a useful model for understanding the relationship between exposure, dose, and effect of nanomaterials in the human lung. It has been shown that the residence time of mineral particles and fibres in the lung depends on their

mechanical clearance and the dissolution rates. The dissolution rate is governed mainly by particle and fibre chemistry and the properties of the biological fluid of the tissue/cell environment in which they are found.
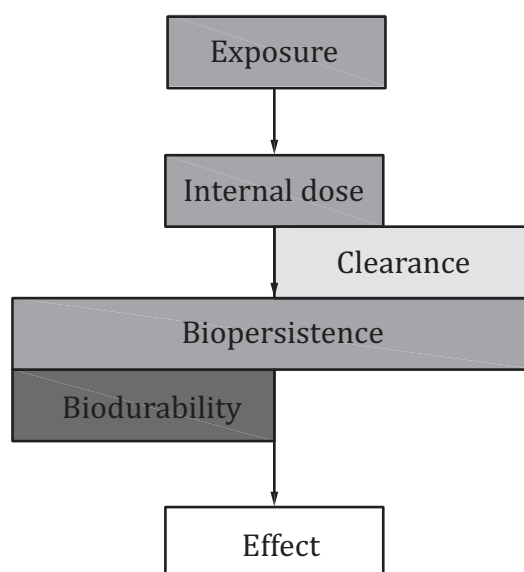
Figure 1 — Relationship between exposure, dose, and effect of nanomaterials[1]

Figure 1 presents a general framework proposed by Oberdörster et al.[1] to evaluate potential adverse effects from exposure to particles and fibres. According to this framework, biopersistence of the particles and fibres is considered to be central to the production of health effects.

The respiratory tract may be divided into different zones, including the ciliated nasal and tracheobronchial regions and the non-ciliated alveolar regions. Particles that deposit in each zone interact with different cell populations with substantially different retention times and/or different clearance pathways[2]. The behaviour of inhaled particles in the respiratory tract and their alternative fates of either deposition or exhalation in these various functional zones may depend upon the chemical composition and the physical behaviour of the aerosol particles.

The importance of airway ciliated cells and alveolar macrophages in the clearance of micrometer-sized particles from the lung surface has long been known. Due to the limited capability of macrophages to recognize nanomaterials, inadequacy of this key clearance mechanism in peripheral lungs was demonstrated[3][4]. Concurrently, due to endocytotic processes and trans-cellular transport mechanisms by other cells, translocation of nanomaterials to extra pulmonary organs has become prominent. Biopersistence of nanomaterials through their resistance to clearance by alveolar macrophages and also to their biodurability through resistance to breakage or dissolution and leaching may therefore lead to their bioaccumulation. With their ability to translocate nanomaterials may accumulate and be retained in critical target organs with the subsequent production of adverse health effects. Translocation (disposition), accumulation and retention are, therefore, important aspects that need to be considered when investigating the long-term toxicity of nanomaterials.

It is now well accepted that the toxicity of nanomaterials may very much be related to their physicochemical properties including size, surface area, and surface characteristics including surface chemistry. Once inside the cell, these and other physicochemical characteristics (surface composition, surface activity) will determine their interaction with biological surroundings. The latter, in turn, will determine the stability and biodurability of the surface and core of nanomaterials. Given the strong sensitivity of many nanomaterial properties to their local environment, it should be noted that biologically relevant changes in the physicochemical properties of a nanomaterial between administration and deposition may have a significant impact on observed responses. As a result,

biodurability of nanomaterials in their local biological environments may impact on their long-term toxicity.

Although the biodurability of certain larger particles can also be confirmed in different environmental media, the importance of such biodurability in their long-term effects might not be of relevance in aquatic organisms. This is shown to be the case with crystalline silica (quartz and cristobalite) for the fact that they do not bioaccumulate in these biorganisms due to their very limited potential for uptake through the gill or gut of fish[5][6]. This might not be true for nanomaterials as the bioaccumulation of multiple-wall carbon nanotubes (MWCNTs) has been shown in *Daphnia magna*, an aquatic invertebrate[7], of gold nanoparticles (AuNPs) in clams marine bivalve *Scrobicularia plana*[8](Pan *et al.*, 2012) and zinc oxide nanoparticles (ZnONPs) in *S. plana* and *Nereis diversicolor*,[9] copper oxide nanoparticles (CuONPs) in freshwater snail[10][11], titanium dioxide nanoparticles (TiO$_2$NPs) in *Daphnia magna*[12], and silver nanoparticles (AgNPs) in deposit feeder such as the annelid *Platynereis dumerilii*[13] have been shown.

6 Aims and objectives

Different nanomaterials are reported to be biopersistent as they resist breakage or dissolution and clearance which in turn can lead to their bioaccumulation and subsequently their translocation and distribution. It is, therefore, of great relevance to assess this property of nanomaterials and determine their degradation half-lives in addition to their other properties. It is also of great relevance to study the impact of surface coating and functional groups on biodurability in biological and environmental surroundings.

The aim and objectives are

— the identification of tests performed and the methodologies implemented in the literature, and

— the description of the identified methodologies in the assessment of the biodurability of different nanomaterials in different biological and environmental media.

The ultimate goal is that, by applying the identified methodologies, it is possible to assess the biodurability of nanomaterials and their surface ligands. This is relevant in the assessment of their long-term effects.

7 Approaches for assessment of micrometre mineral particle and fibre biodurability

7.1 General

The toxicity of inhaled fibres is believed to be related to dose, biodurability and to their dimensions, with long, thin fibres being potentially more carcinogenic than short, thick ones and to their biopersistence, as fibres which dissolve rapidly in the lung are unlikely to induce long-term pathological changes[14]. The concept of biopersistence – resistance to clearance and to chemical dissolution - has therefore been proposed as a key concept in the toxicity of mineral or synthetic fibres.

The critical role of dissolution on the potential health effects of inhaled fibres is well established[15]. Over the last several decades, there have been numerous publications on the relation between various physicochemical characteristics, including chemical composition and diameter, of a synthetic vitreous fibre and its dissolution rate in physiological saline solution[16][17][18].

Numerous animal *in vivo* experiments are described in the literature to assess clearance and chemical instability, through their solubility, of different mineral and man-made synthetic fibres. For example, particle clearance has been studied as a measure of physical persistence - the actual amount of fibre remaining in the tissue and their solubility has been assessed through the release of metal constituents in experimental animals[19][20][21][22][23].

Also, *in vitro* cellular systems have been described to study the chemical stability of particles using macrophages, epithelial, and mesothelial cells where differences could be observed in the efficiency

of these cell types to change the chemical structure of the engulfed fibres emphasizing the differences between phagosomal conditions between these cells[24][25][26][27].

In vitro acellular systems mimicking physiological conditions have been developed to study the release of chemical constituents from fibres. Using different biological media simulants, cell-free chemical dissolution assays were thought to provide valuable information on the behaviour of respired dusts in biological surroundings.

A combination of the *in vitro* dissolution tests, cell-based assays (mono- and co-culture systems), *in silico* methods, and information from existing *in vivo* studies, can provide a measure of biopersistence of mineral particles and fibres. This document is limited to *in vitro* acellular systems and their applications to nanomaterials.

7.2 Dissolution of nanomaterials versus their dispersion and biodegradation

The terms dissolution and dispersion have been defined with a distinction made between these two terms[28]. In this document, dissolution "denotes to the process of obtaining a solution containing the analyte of interest. Dissolution is the act of dissolving and the resulting species may be molecular or ionic" and dispersion "refers to the microscopic multi-phase system in which discontinuities of any state (solid, liquid or gas: discontinuous phase) are dispersed in a continuous phase of a different composition or state". As per this definition, dissolution of nanomaterials will entail release of ions to the surrounding solvent where the rate of dissolution will be dependent on size, chemistry, solvent composition, and surface coating or functionalization of nanomaterials.

Dissolution of nanomaterials is an important property and is often a critical step in determining their safety[29]. Dissolution of metal- and metal oxide-based nanomaterials follows thermodynamic and kinetic rules where size, shape, surface coating, aggregation state, and solution chemistry such as pH, ionic components, and dissolved organic matter (DOM) affect the rate of their dissolution. As the toxicity of the dissolved form can have different toxicological effects than the particulate, monitoring dissolution kinetics is important[30]. Subsequently, the determination of dissolution and dissolution kinetics are recommended as part of the minimum requirements for nanomaterials to be characterized.

Biodegradation of organic and carbon-based nanomaterials on the other hand, is achieved through enzymatic catalysis with subsequent complete breakdown and loss of nanomaterials characteristics. The amenability to biodegradation seemed to be dependent on the type of surface functional groups that they may carry[31].

8 Need for the assessment of nanomaterial biodurability

Biopersistence is one of the characteristics which are seen to determine the toxicity/pathogenicity/ carcinogenicity of ultrafine particles and also of nanomaterials[32]. These characteristics are also seen to alter their fate and biological distribution. Due to their small size, nanomaterials are likely to translocate beyond the epithelial barrier into the interstitium where they accumulate for a long time due to their resistance to phagocytic uptake[33][34][35]. Those which are biodurable may cause pulmonary inflammation, fibrosis, and cancer. Some of the interstitialized nanomaterials could be translocated into the systemic circulation and some may induce impairment in extrapulmonary organs. Once translocated, evidence seems to suggest that nanomaterials preferentially deposit in liver and spleen[36] resulting in prolonged retention and in some instances producing significant hepatotoxicity.

Biodurable nanomaterials maintain their particulate state which might increase the potential for their bioaccumulation[37]. Release of ions from nanomaterials that are soluble have also been shown to be strongly associated with their toxicity while acute toxicological responses arise from nanomaterials with high dissolution through released ions[38], low dissolution and non biodegradable nanomaterials might provoke a range of long-term effects including carcinogenicity[39]. When the sparingly soluble nanomaterials are made soluble through surface functionalization or surface coating, when in contact with body fluids, they might also disintegrate/dissolve to eventually exposing the biodurable core.

9 Influence of different types of ligands and coatings on nanomaterial biodurability

The importance of surface properties of micrometre mineral particles and fibres was recently emphasized as an indirect but critical factor in the manifestation of pathogenic activity as well as in their biodurability under conditions of *in vitro* dissolution in biological fluids. Subsequently, in a publication by the US. National Institute of Occupational Safety and Health (NIOSH), surfaces of mineral particles and fibres were thought to be a controlling factor in their biopersistence, which is seen to be a critical aspect in the mechanisms of continuing irritation or inflammatory response in causing fibrosis or neoplastic transformation[40]. For example, it could be shown that surface composition and surface-associated activities of asbestos fibres were the major contributors to their potential to induce disease. Similar observations have been made for crystalline silica in which surface modification by chemical means has also been shown to alter their cytotoxicity[41][42][43].

Manipulation of surface properties of nanomaterials have also been investigated through surface functionalization with a range of molecular groups for a number of reasons including an increase in water dispersability to an otherwise non-water dispersible nanomaterials and for the increase of their intracellular uptake with their subsequent accumulation in cellular lysosomes. As noted previously, surface chemistry is an important nanomaterial property that will influence interactions with biological fluids. The surface chemistry of nanomaterials can be changed drastically upon immersion in a biological fluid[44]. It is now well recognized that modification of nanomaterial surface chemistry can yield novel properties and behaviours. Such modifications can also be used to promote biodurability and minimize health risks. For example, accumulation in cellular lysosomes could be shown for dextran-coated magnetic iron oxide nanoparticles as well as for single-wall carbon nanotubes (SWCNTs) where they could be enzymatically degraded by lysosomal R-glucosidase, horseradish peroxidase, myeloperoxidase, and heme oxygenase-1. This type of enzymatic degradation, however, might not be possible for inert nanoparticles such as gold and therefore once inside the cell, they can deposit for longer periods[45]. Similar studies with carbon nanotubes (CNTs) have indicated that carboxylated CNTs are more susceptible to biodegradation compared to other CNTs[46].

Loss of ligands from the surface of semiconductor nanocrystals in gastrointestinal fluids at low pH was also reported with the subsequent increase in their toxicity[47]. Moreover, the effect of this biological fluid on the PEGylated quantum dots (QDs) was also investigated and showed that the fate of PEGylated Cadmium-selenium (core) and zinc sulfide (shell) ($CdSe_{core}/ZnS_{shell}$) QDs depended on pH, ligand chain length and presence of proteins and subsequently affecting their toxicity[48][49].

10 Review of methodologies to assess micrometre mineral particle and fibre biodurability

10.1 General

Adaptation of traditional dissolution rate studies to mimic the physical and chemical conditions encountered in biological tissues and organs allows investigators to estimate biodurability through calculation of residence times based on the chemical dissolution mechanism. Particle and fibre dissolution and breakdown in the body are important determinants of their biopersistence. The physical and chemical mechanisms whereby particles and fibres may release ions through dissolution and/or degrade in biological tissues and organs have been studied extensively *in vitro* using "simulated biological fluids" (see Table A.1 to Table A.5). Such *in vitro* tests provide information on the biodurability which impacts the biological effects of particles and fibres[50]. *In vitro* dissolution tests have also been suggested for screening for the biodurability of nanomaterials in environmental media (natural freshwaters, simulated seawater, and simulated estuarine waters) (see Table A.8)[51][52].

10.2 *In vitro* acellular methods

In vitro acellular methods are comprised of two components, the simulated biological fluid and the system to hold and retain the study material. In this first section, various simulated biological fluids are described and in the next section available test systems are reviewed.

Over the last several decades, numerous publications have used various simulated biological fluids to assess dissolution as a measure of biodurability of particles and fibres. Several studies have tried to establish a relation between physicochemical characteristics such as chemical composition, density, and diameter of a synthetic vitreous fibre and their dissolution rate in physiological fluids[53][15]. Several publications have also assessed the impact of different properties of biological fluids on the dissolution of particles and fibres. These properties include pH 7,3 of the extracellular lung fluid and pH 4,5 of macrophage phagolysosomal fluid, presence of surfactants (e.g lung lining fluid), and presence of certain biological compounds, including organic chelators such as sodium citrate that selectively bind to surface ions (see Tables A.1 to A.5).

10.3 Description of different simulated physiological media

10.3.1 General

In this section, simulated biological fluids are described that are intended to mimic the lung and oral as well as dermal exposure pathways. For the lung, generally there are two main compartments to consider – the extracellular airway lining fluid having near neutral pH and the phagolysosomal fluid of macrophage cells having acidic pH. For the oral route, particles will briefly come into contact with saliva followed by gastric and interstitial fluids. To describe adequately the dissolution behaviour of materials in the body, it is imperative that the simulant reflects the biochemical composition of the fluids in the organ or tissue being modelled. The most common simulants used were therefore based on the ionic composition of lung extracellular fluid described by Gamble[54] which is near neutral pH (7,2 to 7,4). Gamble's simulant fluid was also called Ringer's solutions, simulant ultrafiltrate fluid (SUF), or simulant lung fluid (SLF)[55][56]. The majority of experiments have, therefore, been conducted at physiological pH (7,3), either at 25 °C or 37 °C. With evidence that dissolution of insoluble particles occurs predominantly in phagolysosomes, investigators began to adjust the pH of lung extracellular fluid-simulants to match that of the phagolysosome, i.e. pH 4,5 to 5.

Therefore, the simulated physiological fluids (SPF) that are discussed below have included: (1) the lung airway lining simulant, (2) the phagolysosomal stimulant fluid, (3) the simulated saliva, (4) the gastrointestinal fluids, as well as (5) sweat the composition of all of which are presented in Annex A. For more information on the composition of various biological fluids and their simulants, the reader is referred to Marques et al.[57].

While these SPF are considered useful analogues of human biofluids, they all suffer from the same basic limitations. Firstly, SPFs have defined compositions and lack the dynamic conditions present *in vivo*. For example, none of these fluids contain enzymes or oxidative cascades which can be important in dictating the properties (composition, pH) of a SPF or biodurability of nanomaterials such as carbon nanotubes[58]. Additionally, unless specifically noted, proteins are omitted from most SPF for pragmatic reasons (see 10.5.3); however, *in vivo*, proteins might serve as important binding molecules for dissolved ions and influence their concentration at nanomaterial surfaces.

10.3.2 Simulated lung airway lining fluids

Aerosol materials that deposit in the lung are quickly immersed in the extracellular fluid that is excreted by the lung tissue. The original composition of physiological fluids described by Gamble in 1967[54] has served as a basis for a number of experimental derivations for human extracellular fluid, including the experimental solvents used by Scholze and Conradt[59] and Kanapilly et al.[60].

Gamble's Solution is a type of simulated lung airway lining fluid that is intended to mimic the surfactant fluids released by Type II alveolar cells. The fluid fills the space between alveolar cells and acts to reduce the surface tension of the water in the lungs, facilitating gas exchange. The composition of this solution was compared to the fluid in human lungs and found to be identical in terms of major components. The original Gamble's Solution was a mixture of water and inorganic salts including chlorides, carbonates and phosphates. Most researchers have however modified the solution to include proteins and other organic components, chelators and additives[61] (see Table A.1).

10.3.3 Simulated lung macrophage phagolysosomal fluid

Particles that deposit in the non-ciliated alveolar region of the lung are initially immersed in extracellular airway lining fluid but are rapidly phagocytized by scavenger cells such as macrophages. Upon engulfment by a macrophage cell, the particle-laden vesicle (lysosome) fuses with a phagososome to form a phagolysosome which is rich in oxidizers and has acidic pH to promote degradation of foreign materials.

The original composition of SPF described by Gamble in 1967[54] served as a basis for human macrophage phagolysosomal fluid (PSF). The fusion occurs when neutrophil or macrophage encounters a foreign substance, including nanomaterials, with ensuing destruction or degradation of the foreign substance in the phagolysosome. The intracellular fluid within alveolar macrophages is considerably more acidic (pH approximately 5 to 6) than the extracellular fluid (pH approximately 7 to 7,5). Some particles that do not dissolve efficiently in extracellular lung fluid are degraded within the cellular phagolysosomes of alveolar macrophages[62][63][64][65][66][67][46][68][69] (see Table A.2).

10.3.4 Digestive system (saliva, gastric and intestinal fluids)

10.3.4.1 General

The main fluids of the digestive system may include saliva, gastric and intestinal fluids[57][70]. The stomach produces gastric juice while the intestine is a mixture of bile from liver (digestive enzymes) and pancreatic juice. The assessment of biodurability in these fluids may be of relevance when considering the development of nanomaterials for drug delivery or for mouth cleansing formulations[71][72].

10.3.4.2 Simulated saliva (SS)

It is almost impossible to duplicate the properties of human saliva because of its particular characteristics. Saliva is a mixture of fluids secreted by several salivary glands, with numerous constituents, which varies depending on time of day and diet. The pH of the normal healthy saliva is between 6,7 to 7,4 which may drop to pH 5 when sweets and carbohydrates are consumed. Simulated saliva (SS) was developed for different applications[73][74][75][76] (see Table A.3) and was also used to test the dissolution of nickel nanoparticles[77].

10.3.4.3 Simulated gastric fluid

Conditions in the gastric environment, such as pH, enzyme concentration, water content, temperature, pressure, microbial load, and emptying rate are continually changing during the fasting and fed states[78][79]. Acellular *in vitro* digestion assays using simulated gastric fluids (see Table A.4) have been used to determine how human gastric conditions impact the behaviour of nanomaterials. For example, AgNPs in simulated gastric fluid aggregated significantly and released ionic silver from their surface that re-precipitated and coated the aggregates as silver chloride[80][81]. The aggregation rate was higher for smaller (10 nm) AgNPs compared with larger (75 nm) nanoparticles (NPs). Additionally, the ionic silver released from the NPs could generate new AgNPs that might differ in size and morphology from the NPs that the system was initially exposed to[82][83]. The low pH of the gastric fluid could also cause degradation of the surface coating of nanomaterials, which could alter their downstream toxicity[70][84]. These studies demonstrate the importance of using isolated acellular systems such as gastric fluids to understand behaviour of nanomaterials in these fluids. In addition to exposing nanomaterials to simulated gastric fluids separately, there are systems that simulate sections of the gastrointestinal system, from the mouth to intestine, to allow sequential exposure of test materials to different compartments[78][85]. These systems can be useful in studying how nanomaterials are affected by different conditions that change substantially from one compartment to another.

10.3.4.4 Simulated intestinal fluid

The fasted-state simulated intestinal fluid and fed-state simulated intestinal fluid (see Table A.4) were introduced to simulate additional important aspects of the GI fluids, including bile salts and lecithin[71].

10.3.5 Simulated sweat (SSW)

The surface of the skin is coated with a co-solvent of mainly aqueous sweat and oily sebum. Human sweat contains over 60 different constituents and because of this complexity, most simulated sweats have been greatly simplified for use with *in vitro* tests. Further, it is very difficult to disperse oily sebum constituents in aqueous sweat to mimic the co-solvent behaviour on the skin surface. As such, most investigators evaluate biodurability in either simulated sweat or sebum. Human sweat pH varies with anatomical region which is an important consideration when designing *in vitro* dissolution studies. For healthy adults, skin surface pH is generally in the range of 4,2 to 6,1[86]. The most commonly used simulated sweat is a simple formulation developed by Pedersen et al.[87], though more recently a simulated sweat having composition that more accurately mimics human sweat has been developed[88]. Sebum contains several lipids and antioxidants such as vitamin E. Formulations of simulated sebum vary from a single constituent[89] to containing multiple types of lipids representative of human sebum composition[90][91][92]. Since 1940, there have been at least 76 different simulated sweat formulations and 27 different simulated sebum formulations used with *in vitro* test methods[93] (see Table A.5).

10.4 Description of different simulated environmental media

10.4.1 General

Different environmental media such as natural freshwater, simulated seawater, and simulated estuarine waters, were also used to assess the dissolution of nanomaterials[52][94].

10.4.2 Simulated natural freshwaters

For dissolution studies of nanomaterials in simulated natural waters,[52] the composition recommended by United States (US) Environmental Protection Agency (EPA) was implemented[51] (see Table A.6). The preparation of such simulated fluids of these natural waters with different hardness was also described[95]. Using these simulated media, the dissolution of ZnO nanoparticles in a freshwater medium (pH 7,6) was assessed[30].

10.4.3 Simulated seawater

For dissolution studies in simulated seawater[52], the composition recommended by EPA[51], based on GP2 artificial sea water medium[96] as well as by others[95] was implemented (see Table A.7). Using simulated sea water, the dissolution kinetics of commercial uncoated and organic-coated ZnONPs[97] and also AgNPs[52] were investigated.

10.4.4 Simulated estuarine waters

The biodurability of citrate-capped 20 nm AgNPs was also investigated in simulated estuarine waters (see Table A.8) where the stability and hence biodurability of these nanoparticles in fresh waters could be confirmed. The importance of understanding the colloidal stability of AgNP dispersions was, therefore, emphasized to enable better prediction of their persistence in environmental waters and their subsequent toxicity[52].

10.5 Description of different test systems to assess dissolution of particles and fibres

10.5.1 General

Geochemists have developed methodologies to assess dissolution rate of mineral substances as a measure of weathering in the environment. These methodologies were later adapted to describe the biodurability of hazardous mineral particles and fibres. It has, therefore, been stipulated that the *in vitro* dissolution techniques provide a simple, cost-effective methodology by which dissolution rates of particles and fibres can be estimated. As such, these techniques have been implemented as a screening methodology for their biodurability. The systems implemented have included: (1) static dissolution system, (2) parallel-flow system, (3) batch system and batch filter system, (4) flow-through

dissolution system, and (5) continuous flow system. The description of mathematical modelling used in the assessment of the dissolution of nanomaterials implementing some of these methodologies was recently presented[98].

Each of these five test systems has unique advantages and disadvantages for evaluation of biodurability. Specific discussions of the appropriateness of a technique for evaluation of nanomaterial biodurability are discussed in the ensuing subsections.

10.5.2 Static dissolution system

In this system[61], the particle samples are confined between two 0,1 μm or down to 0,025 μm pore size membrane filters membrane to form a sandwich, which are then secured between two tight-fitting polypropylene rings. The purpose of the rings is to form the chamber and a rubber o-ring is used to form a particle tight seal and prevent solid materials from accessing the liquid and being quantified as dissolved. The sample holder is then placed in a beaker and sufficient solvent is added to cover the assembly and thus exposing the samples to the solvent on both sides of the filters. After a selected time interval, the solvent is removed and the concentration determined in the solution. An equivalent volume of fresh solvent is added to the filter assembly and the process is repeated. This test, which is among the easiest to implement, has been widely used by different authors[60]. Dissolution rates can then be assessed either from changes in sample mass or by monitoring chemical changes in the experimental fluid. A major limitation of this system is the possibility of the supernatant to become supersaturated with one of the solute species, and thus inhibiting further dissolution as well as the solute build-up on the surfaces of the particles tested with subsequent reduction in dissolution rate[99]. As such, use of this technique may be more appropriate for poorly soluble nanomaterials but not for highly soluble nanomaterials such as zinc oxide. Despite these limitations, the dissolution studies of some nanomaterials can be conducted with a static dissolution system[100][101].

10.5.3 Continuous flow system (CFS)

Due to potential problems of supersaturation that can arise in static experiments (see 10.5.2), the continuous flow system (CFS) protocol is seen to be the best method of measuring durability *in vitro*[102]. In this methodology, using a peristaltic pump, the simulated fluids from a large reservoir is pumped through a cell containing the particle sample. The dissolution rate is then assessed through measurement of solute concentrations in the fluid after it has passed through the cell[99]. Using this system, a number of *in vitro* dissolution studies were conducted to assess the biodurability of micrometre-scale particles and fibres[103][104][105]. It must be noted that while implementing this system, proteins in simulated biological fluids can clog the pores in filters causing rupture of samples[61]. Additionally, the CFS technique can require large volumes of simulated biological fluid which might be problematic for waste generation, especially if evaluating radiolabelled nanomaterials.

10.5.4 Batch and batch filter systems

In this system, the sample of particles is shaken, usually in a centrifuge tube, with a solvent under controlled temperature conditions for a selected time interval. The mixture is then centrifuged at specified time intervals and an aliquot of the supernatant solution is withdrawn and then analysed. The aliquot volume is/should be replaced with fresh solvent to maintain a constant dilution volume. The direct contact between dust and solvent eliminates possible matrix effects attributable to the presence of membrane filters. In the batch filter system, the same is applied with the exception that the solution is filtered through a membrane filter with the advantage of not being as susceptible to particle transfer into the measurement aliquot. Limitations of these techniques include the potential artefact on dissolution from shaking and the potential for soluble nanomaterials to continue to dissolve during centrifugation (see 10.6.3.2).

10.5.5 Tangential flow filtration system

Recently, a unique diffusion-driven filtration method was implemented which is able to retain large particles within the continuous flow path, while allowing constituents smaller than the membrane pore size (ions) to pass through molecular filters by lateral diffusion separation. To separate the

nanoparticles from the solvated ions, the solution is passed through a membrane with pore size of 10 kDa, which is rinsed prior to filtrations with 70 % isopropanol to create a hydrophilic surface on the membrane. After filtration, the concentration of the ions is then quantified using inductively coupled plasma-mass spectrometry (ICP-MS). It is said that this system has a number of advantages of the previously described systems implementing centrifugation, filtration or dialysis [83].

10.6 Assessment of dissolved mass concentration post dissolution experiment

10.6.1 General

The most common methods used to measure the concentration of ions from dissolution of nanomaterials include ICP-optical emission spectrometry (ICP-OES), ICP-mass spectrometry (ICP-MS), atomic absorption spectroscopy (AAS), and laser post-ionization secondary neutral mass spectrometry/time-of-flight secondary ion mass spectrometry (Laser-SNMS/TOF-SIMS)[106].

Generally, these methods provide a quantitative measure of total elemental concentration in a sample of simulated physiological media and cannot discriminate between an element in dissolved form or in particulate form. Hence, depending on the test system used, prior to quantification of dissolved forms, it might be necessary to subject samples to a separation (also called fractionation) procedure to isolate the analyte of interest from the nanomaterial of interest and other elemental ions. There are a variety of different separation techniques available and they can be broadly categorized based on their operating principle (physical, mechanical, or chemical). These techniques vary in cost, complexity, and efficiency. The choice of separation technique is an important component of any biodurability study design because, depending upon the ions or molecules of interest, the simulated physiological fluid composition, and the separation procedure, this step may be a source of potential artefacts.

10.6.2 Techniques based on physical principles

Techniques based on physical principles for separation include flow field flow fractionation (FFFF)[107] [108] and size exclusion chromatography[109][[110].

10.6.2.1 Flow field flow fractionation

Flow field flow fractionation is a general term for a group of techniques that, analogous to chromatography, rely on elution times for separation of nanomaterials by particle size. Depending upon the system, materials can be separated with high resolution over a broad range of sizes, from 1 nm to 100 μm[111][112]. There are two main variations of this technique, symmetric FFFF and asymmetrical flow field flow fractionation (AF4)[111][113]. In FFFF, a suspension is introduced into an elongated ribbon-like channel with an ultrafiltration membrane on one side. Because of the high aspect ratio of this chamber, the suspension (carrier liquid) develops parabolic laminar flow toward the outlet of the chamber. A cross-flow is applied perpendicularly which pushes particles toward the membrane. As the particle concentration along the membrane wall of the chamber builds up, the particles diffuse back into the flow of the chamber and become aligned with the streamlines of the parabolic flow according to their hydrodynamic size (smaller particles align at the apex of the parabola and are eluted faster than larger particles which align at the edges of the parabola near the chamber wall where velocity is much slower). The operating principle of AF4 is similar, though in this technique, a trapezoid-shaped channel is used. For both FFFF and AF4, the type of ultrafiltration membrane and its potential to interact with dissolved and/or particulate material in a simulated physiological or environmental fluid is an important consideration. Reference [114] systematically evaluated the main parameters that directly influence the separation of AgNPs with AF4 and identified the channel spacer thickness, flow conditions, eluent (pH, composition, temperature, viscosity), membrane material and the properties of the nanomaterial itself (surface chemistry/coatings) as important factors.

10.6.2.2 Chromatography (size exclusion, hydrodynamic)

High-performance size exclusion chromatography (HPSEC) is a powerful tool for probing the size and size distribution of complex materials[115][116].

10.6.3 Techniques based on mechanical concepts

Techniques based on mechanical concepts have included the use of membranes and also centrifugation.

10.6.3.1 Membranes

Porous membranes are often utilized to separate and concentrate dissolved forms from particulate material and/or other dissolved ions. Donnan dialysis is an ion exchange technique that is based on establishing electrochemical and ion transport equilibriums between two solutions separated by a membrane. The membrane can either be a cation exchange membrane or an anion exchange membrane. Initially, a high concentration of the ion of interest is present in a sample on one side of a membrane and absent from the receiving solution on the other side of the membrane. Over time, ions of interest diffuse across the membrane into the receiving solution and are exchanged for the same amount of ions of a different analyte until equilibrium is achieved. The receiving solution is then quantified for the amount of ion of interest. Donnan dialysis[117] has been used to separate a wide range of metal ions including gold, palladium, platinum, and iron[118]. The advantage of Donnan dialysis, which utilizes counter diffusion or more ions through an ion exchange membrane to achieve separation, is that it is a simple and cost effective technique; however, it might take several hours to reach equilibrium and, depending upon the ion and membrane, there is potential for ion adsorption onto the membrane which can bias results.

Centrifugal filtration is a membrane-based technique that can be used to separate dissolved ions from particulate nanomaterials[46]. In this technique, a dilute aqueous sample is added to a centrifuge tube that contains an ultrafiltration membrane and centrifuged (typically at 4 000 × g or 5 000 × g). The dissolved ions pass through the membrane and are concentrated in the ultrafiltrate and the particulate material is retained on the membrane. Most commonly, ultrafiltration membranes with nominal molecular weight cut-offs of 3 000 Da to 10 000 Da are used for separation of nanomaterials. There is no direct conversion from Daltons (a three-dimensional molecular size) to nanometers, though these membranes correspond to nanomaterial sizes of approximately 1 nm to 3 nm. Centrifugal filtration offers several advantages, including cost effectiveness and the ability to separate nanomaterials in suspension without the need for ultracentrifugation. However, depending on the type of membrane and its potential to interact with dissolved ions, the element of interest may adsorb to the membrane and introduce bias[114][119].

10.6.3.2 Ultracentrifugation

Ultracentrifugation can be used to separate dissolved forms from particulate nanomaterial. This technique uses centrifugal force to move nanomaterials through an aqueous suspension to the bottom of a centrifuge tube. The end result is a pellet of solid nanomaterials and liquid supernatant that contains dissolved ions. The terminal settling velocity (V_{TC}), in units of cm s^{-1}, for a particle subject to centrifugal force is described by Formula (1):

$$V_{TC} = \frac{Cc\rho_p d^2 a_c}{18\eta} \tag{1}$$

where

Cc	is the Cunningham correction factor or slip correction factor;
ρ_p	is the particle density;
d	is the particle diameter;
a_c	is the centrifugal acceleration at the particle;
18	is the constant;
η	is the viscosity of the liquid.

The centrifugation time to move a nanomaterial a given distance can be calculated from the ratio of the distance needed to move the particle and V_{TC}.[120] From Formula 1, it is evident that because of their small size, very high centrifugal forces and long times are needed for separation of nanomaterials[119][121][122]. As such, ultracentrifugation is only applicable for separation of poorly soluble nanomaterials and not highly soluble nanomaterials which would continue to dissolve during the separation process.

10.6.4 Techniques based on chemical principles

To date, a variety of approaches such as liquid-liquid extraction, solid-liquid extraction, cloud-point extraction, and coated magnetic particles have been developed for extraction and concentration of NPs.

10.6.4.1 Liquid-liquid extraction

Liquid-liquid extraction is a very common method by which a compound is pulled from one solvent to another where these solvents are not miscible. Using this methodology, several nanomaterials were extracted from aqueous solutions to organic solvents through varying their surfaces from hydrophilicity to hydrophobicity using surfactant modification[123][124][125][126][127][128].

10.6.4.2 Solid-phase extraction (SPE)

Solid-phase extraction (SPE) is a useful technique to separate the analyte of interest from matrix interferences. This technique has the added benefits of being able to pre-concentrate, does not alter solution chemistry, nor does it require the additional step of removal of undissolved nanomaterials before analysis as with ultrafiltration or ultracentrifugation[129][130]. In this technique, the solubilized analyte of interest is reversibly bound and retained on a selective solid phase sorbent substrate (solid phase extraction) or on a substrate coated with a selective sorbent (solid phase microextraction). The sorbent can be packed in a cartridge over which the suspension is passed, a probe such as a fibre is inserted into the suspension, or even a nanomaterial such as graphene[131] or functionalized magnetic nanoparticles[130][132][133] that is introduced directly into the suspension. Once ions are adsorbed onto the sorbent they are eluted from the solid phase substrate using an appropriate liquid and analysed by an applicable technique such as gas chromatography–mass spectrometry (GC-MS), liquid chromatography-mass spectrometry (LC-MS), high-performance chelation ion chromatography (HPCIC), ICP-MS, etc.

10.6.4.3 Cloud-point extraction (CPE)

CPE has been used for separation and concentration in studies of several different nanomaterials including silver[134][135] and gold, titanium dioxide, iron oxide, C_{60} fullerenes, SWCNTs, and $CdSe_{core}/ZnS_{shell}$ quantum dots[136]. Briefly, this technique involves the mixing of an aqueous sample with appropriate chemicals and a surfactant, incubation to promote phase separation, and centrifugation. The result is a two phase sample with the surfactant rich phase that contains the nanomaterial of interest on the bottom of a centrifuge tube and the aqueous phase that contains the ions of interest in the supernatant. CPE has been demonstrated to be robust for silver nanomaterials with a variety of different surface coatings and a range of waters containing organic and inorganic constituents[134] and several metals, metal oxides, and carbon-based materials[136] which make it a useful technique for biodurability studies in simulated environmental and physiological fluids.

10.6.4.4 Coated magnetic particles

This technique involves the use of magnetic iron oxide nanoparticles coated with dopamine or glutathione to selectively capture and bind silver in particulate[137]. Briefly, coated iron oxide nanoparticles are mixed with an aqueous sample that contains silver nanomaterials, shaken, and incubated to facilitate absorption of silver to the magnetic nanoparticles. The suspension is passed through a cell with an inlet and an outlet and a magnetic field is applied to remove and capture the iron oxide nanoparticles with silver nanomaterials bound in particulate form. The cell eluent contains silver in the form of ions only. The efficiency of this technique is reported to be >99 %.

### 10.6.5 Ultraviolet-visible (UV-Vis) spectroscopy

Due to concerns with these conventional systems [membranes, ultracentrifugation and capillary electrophoresis (CE)] of separation in environmental waters and culture media with low salt concentrations, the use of UV-Visible spectroscopy was recommended for nanomaterials that have surface Plasmon resonance (SPR)[138]. However, solutions with high concentrations of chlorides result in adsorption of silver chloride on AgNPs surfaces[139]. Because silver salts do not exhibit SPR, UV-visible absorbance spectroscopy might have limited ability to detect silver nanoparticles in these types of solutions[140].

10.6.6 One-dimensional mathematical models

Most recently, a one-dimensional mathematical model was developed and implemented to describe the coupled transport of citrate-stabilized AgNPs and dissolved silver ions in porous media[141].

10.6.7 Single particle inductively coupled plasma-mass spectrometry (spICP-MS)

When analysing dissolved samples with ICP-MS, a steady-state signal results from measuring dissolved element. With single particle inductively coupled-mass spectrometry (spICP-MS), both dissolved elements and particles are measured. This is for the fact that with the former, when aerosols enter the plasma to be desolvated and ionized, the resulting ions enter the quadrupole to be sorted by their mass-to-charge ratios (m/z). The quadrupole spends a certain amount of time (dwell time) at each m/z followed by a stabilization time (settling time) before moving to the next m/z. During the settling time of the electronics, significant amount of the signal is not measured which might not be of significance for dissolved ions which produces a continuous signal; this could however be critical for suspended particles. Therefore, by increasing the transient data acquisition speed with the elimination of the settling time between measurements to enable continuous data collection without any settling time, it will be ensured that every particle entering the plasma is counted with the possibility of measuring multiple points per single particle and thus eliminating the chances that particles are missed for precise nanoparticle counting and sizing (Figures 2 and 3).
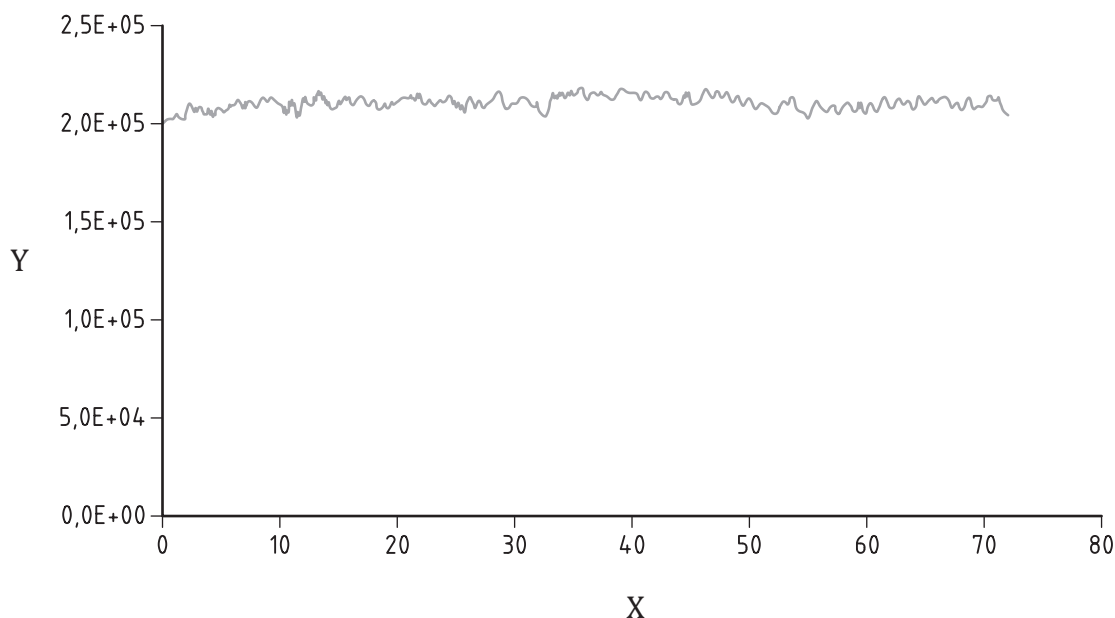
Key

X   time/min

Y   intensity/cps

Figure 2 — Steady-state signal from dissolved analyte (>1 hour)
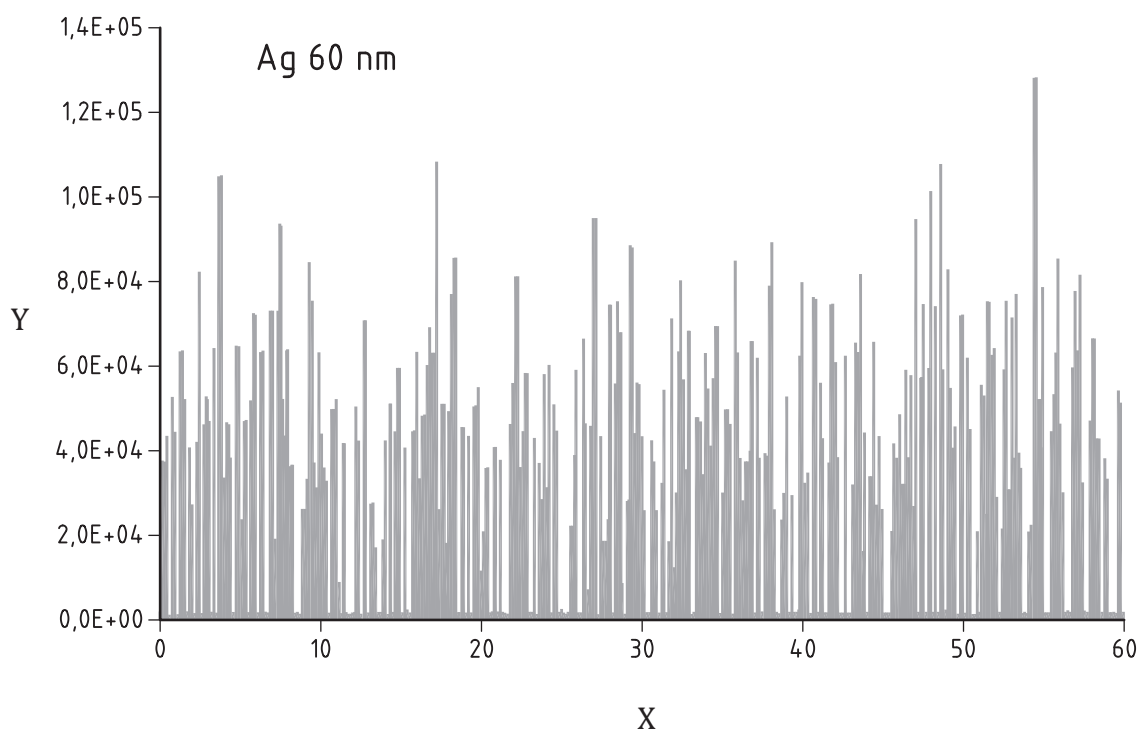
Key

X   time/s

Y   intensity/cps

Figure 3 — Steady-state signal from dissolved analyte (1 min., where each spike represents a particle)

Using this technology, the dissolution of nanoparticle could be measured primarily as a decrease in particle diameter as the metric of dissolution over time but also with direct measurement of released Ag+[142][143][144][145][146][147].

11 Calculation of micrometre mineral particle biodurability

11.1 General

Biodurability of particles and fibres is assessed through the determination of their halftimes and lifetimes.

The identification of the dissolution kinetics and the subsequent calculation of dissolution rates and dissolution rate constants are in turn, the necessary parameters for the calculation of particle biodurability.

11.2 Dissolution kinetics, dissolution rates, and dissolution rate constants

Dissolution kinetic studies are implemented to determine the dissolution rates and dissolution rate constants of particles and fibres. It has been shown that larger particles release ions in zero order kinetics. In general, for a zero order reaction, the reaction rate is defined as Formula (2):

$$\text{Rate} = -\frac{\Delta[M]}{\Delta t} = -\frac{dM}{dt} = k[M]^0 \tag{2}$$

where

ΔM is the change of mass of the reactant within the time interval Δt;

$\Delta t, M^0$ is the concentration of the reactant;

t is the time of the reaction and the rate of reaction is equal to the rate constant, k, and, therefore, is independent of the original mass of the reactant.

It has also been shown that the dissolution of ions with most nanoparticles follow first order kinetics. For a first order kinetics, the reaction rate is defined as Formula (3):

$$\text{Rate} = -\frac{\Delta[M]}{\Delta t} = \frac{dM}{dt} \tag{3}$$

But the reaction rate is expressed as:

$$-\frac{dM}{dt} = k_{\text{diss}}[M] \tag{4}$$

where the reaction rate is again dependent on rate constant k_{diss}, but also dependent on M, the mass of the reactant [see Formula (4)].

11.3 Dissolution kinetics and dissolution rate of larger particles and fibres

The dissolution of particles was initially described by Mercer[148]. The dissolution kinetics, rate and rate constants were later studied in more detail *in vitro*. For larger particles and fibres where the dissolution rate is said to follow a zero order reaction, the dissolution rate is shown to be independent of mass but is a function of its dissolution rate constant and a function of its surface area, *A.* It is also said to be dependent on the solvent, the diffusion of atoms or molecules through the stagnant layer of solvent around the particle or the diffusion to the surface of the more soluble component of a multicomponent particle[149][150].

The dissolution rate of a solid with a zero order reaction can then be expressed as Formula (5):

$$\frac{dM}{dt} = -Ak_{\text{diss}} \tag{5}$$

where

A is the surface area of the particle and k_{diss} is the dissolution rate constant.

However, the basic principle for particle dissolution[61], which was originally described by Mercer[148], is that the dissolution rate of a solid is a function of its specific surface area, *S*. Subsequently, with

substituting the surface area with specific surface area S of the particle, the dissolution rate was then expressed as Formula (6):

$$\frac{d\left(\dfrac{M}{M_0}\right)}{dt} = -k_{\text{diss}}S(t) \tag{6}$$

where

M/M_0 is the normalized undissolved mass;

k_{diss} is the dissolution rate constant (mass/area/time);

S is the specific surface area (surface area/mass);

t is time.

Initially, S is said to be a function of particle size distribution and particle shape factor[148], but it changes as dissolution progresses, such that S is a function of time, $S(t)$.

The dissolution of fibres, similar to the dissolution of silica based microparticles, has been described by the surface area normalized zero[th] order kinetic dissolution rate law where the dissolution are commonly quantified using the parameter k_{dis} and is expressed in units of ng/cm^2/h. It is generally assumed that the rate of mass loss from fibres (M) is proportional to their surface area (A) and independent of time (t)[99]. With fibres however, with the assumption of cylindrical-shaped fibres with uniform diameter dissolving congruently from an initial mass, M_0, and initial diameter, d_0, the solving of the surface area normalized zero[th] order kinetic dissolution rate law can be represented as Formula (7):

$$1 - \left(\frac{M}{M_0}\right)^{\frac{1}{2}} = \frac{2k_{\text{diss}}t}{d_0\rho} \tag{7}$$

where

ρ is the initial fibre density.

These two formulae can be solved to a formula which relates the fibre diameter, d, at time, t, to the initial fibre diameter, d_0, density of the fibre, ρ, and the dissolution rate constant, k_{diss}, in Formula (8)[15]:

$$d(t) = d_0 - \frac{2k_{\text{diss}}t}{\rho} \tag{8}$$

where

k_{diss} is measured in units of mass/area/time;

D is the fibre diameter at time, t;

d_0 is units of length such as cm;

ρ is g/cm^3.

11.4 Dissolution kinetics and dissolution rate of nanoparticles

The dissolution of most nanoparticles is shown to follow a first order kinetics[92][151] and, therefore, the dissolution rate will be dependent not only on the dissolution rate constant, k_{diss}, and on their specific surface area, S, but also on mass. This relationship is, therefore, represented as Formula (9):

$$\frac{dM}{dt} = -k_{diss}M \tag{9}$$

Similarly, it is said that the dissolution rate of smaller particles is proportional to their surface area, but the dissolution of small particle should be faster according to the Noyes-Whitney equation [see Formula (10)]:

$$\frac{dm}{dt} = \frac{DA}{h}(c_s - c) \tag{10}$$

where

dm/dt	is the dissolution rate;
D	is the diffusion coefficient;
A,	is the surface area;
h	is the thickness of the diffusion layer;
c_s	is the saturation concentration;
c	is the bulk concentration.

11.5 Assessment of halftime estimates of particles and fibres

For zero-order processes, the halftime of particles or fibres can be calculated with Formula (11):

$$t_{1/2} = \frac{[\text{reactant}]_0}{2k_{diss}} \tag{11}$$

where

[reactant]$_0$	is the initial concentration of the substance;
k_{diss}	is the dissolution rate constant (mass/area/time);
$t_{1/2}$	is the halftime.

For a zero-order reaction, the halftime decreases with decreasing initial concentration. Therefore, halftime for substances that dissolve by zero-order kinetics are not very useful.

Formula (12) was therefore used to determine the halftime of fibres with zero order kinetics:

$$1 - \left(\frac{M}{M_0}\right)^{\frac{1}{2}} = \frac{2k_{diss}t}{D_0\rho} \tag{12}$$

where $1-(M/M_0)^{1/2}$ is plotted against time nonlinear least squares regression modelling will yield $t_{1/2}$ and the dissolution rate constant, k[92].

For first-order kinetics, rate constants and half-lives represent the same process and are inversely related as represented by Formula (13)[153]:

$$t_{1/2} = \frac{\ln(2)}{k_{\text{diss}}}$$ (13)

where

$t_{1/2}$ is the halftime/life (in units of time);

k_{diss} is (the non-normalized) dissolution rate constant (1/units of time).

11.6 Assessment of lifetime estimates for particles and fibres

11.6.1 General

For dissolution of particles and fibres that follow zero order kinetics, two variant models are used for establishing their lifetime.

11.6.2 Shrinking sphere theory

For particles, the particle lifetime estimates as modelled using a "shrinking sphere" geometry where the time to dissolve the sphere is defined by the diameter of the particle[153].

Using the zero$^{\text{th}}$ order rate law which can also be expressed in terms of number of particles (n) instead of mass (M) [Formula (14)]:

$$\frac{dn}{dt} = -Ak_{\text{diss}}$$ (14)

and with the consideration of the surface area of a sphere as $4\pi r^2$ and considering the volume of a sphere as $V = \frac{4\pi r^3}{3}$, the A in Formula (14) can then be expressed as Formula (15):

$$A = Vb^{2/3}$$ (15)

which can then be rearranged as Formula (16):

$$\frac{4\pi r^2}{3} = b\left(\frac{4\pi r^3}{3}\right)^{\frac{2}{3}}$$ (16)

The value of b can then be solved to be equal to 4,84.

The volume, V of a material is defined as Formula (17):

$$V = nV_m \tag{17}$$

where V_m is the molar volume of a substance and n is the number of moles [see Formula (18)].

$$A = bn^{2/3}V_m^{2/3} \tag{18}$$

The value A derived above is then substituted in the zeroth order rate law above. The formula will then be expressed as Formula (19):

$$\frac{dn}{dt} = -bV_m^{2/3}k_{diss}n^{2/3} \tag{19}$$

With further derivation, the formula will then be expressed as Formula (20):

$$\Delta t = \frac{r}{V_m k_{diss}} \tag{20}$$

Substituting for $r = d/2$ (see Formula 21),

$$t = \frac{d}{2k_{diss}V_m} \tag{21}$$

where

t is time (sec),

d is the particle diameter (m),

V_m is the molar volume (m^3/mol)

k_{diss} is the rate constant (mol/surface area/time).

11.6.3 Shrinking fibre theory

Using the same zeroth order rate law once again expressed in terms of number of particles (n) instead of mass (M) (see Formula 22):

$$\frac{dn}{dt} = -Ak_{diss} \tag{22}$$

but with the assumption of a cylindrical shape for fibres, the lateral surface area (A) of a cylinder is given by $A = 2\pi r l$ and its volume is given by $V = \pi r^2 l$ where r is the radius of the cylinder and l is its length with the aspect ratio (z) of the cylinder to be defined as $z = r/l$ so that $r = l/z$.

Assuming cylindrical-shaped fibres and that dissolution affects only the diameter of a fibre (not its length), this model can be written as shown below (see Formula 23):

$$d_t = d_0 - \frac{2k_{diss}t}{\rho} \tag{23}$$

The lateral surface area (A) will then be $A = 2\pi l^2 z$ and $V = \dfrac{\pi r^3}{z}$.

The general relationship between the surface area of a solid and its volume will subsequently be expressed as Formula (24):

$$A = Vb^{2/3} \tag{24}$$

where b value is equivalent in Formula (25):

$$b = 2\frac{\pi^{1/3}}{z^{1/3}} \tag{25}$$

Once again, the volume of material V can be defined as Formula (26):

$$V = nV_m \tag{26}$$

where n is the number of moles of substance in the cylinder and V_m is the molar volume. The A in Formula (24) can then be expressed as Formula (27):

$$A - \frac{2\pi^{1/3}V_m^{2/3}n^{2/3}}{z^{1/3}} \tag{27}$$

When the value of A is substituted in the zero[th] order law, the formula can then be expressed as Formula (28):

$$\frac{dn}{dt} = -\frac{2\pi^{1/3}V_m^{2/3}k_{\text{diss}}n^{2/3}}{z^{1/3}} \tag{28}$$

With further integration and rearrangements, the formula is expressed as Formula (29):

$$t = \frac{3n^{1/3}z^{1/3}}{2\pi^{1/3}V_m^{2/3}k_{\text{diss}}} \tag{29}$$

and with further substitution of n and z as per earlier definitions, the formula is then represented as Formula (30):

$$t = \frac{3r}{2V_m k_{\text{diss}}} \tag{30}$$

which gives the time to dissolve a fibre of radius, r.

With the definition of fibre dimensions that $r = \frac{d}{2}$, Formula (30) can then be written in terms of the diameter of the fibre as Formula (31):

$$t = \frac{3d}{4V_m k_{\text{diss}}} \tag{31}$$

11.7 Assessment of halftime and lifetime estimates

Using these two models, lifetime estimates for number of particles and fibres could be calculated using Formula (21) for particles and Formula (31) for fibres as presented in Table 1[50][68][153][154][155][156][157][158].

Table 1 — Halftime (calculated from k_{diss}) of nanoparticles with dissolution of first order kinetics and lifetime (estimated from shrinking sphere/fibre model) of nano and microparticles and fibres with zero order kinetics

Mineral particles/fibres	k_{diss}	Halftime	Lifetime
Larger particles and fibres			
WO$_3$, aggregated 36,2 μm, in artificial airway epithelial lining fluid (pH 7,4)	$2,5 \pm 0,3 \times 10^{-5}$ g[a] tungsten/cm^2/day[68]	4 d ± 1 d	
WO$_3$, individual 36,2 μm in artificial airway epithelial lining fluid (pH 7,4)	$0,9 \times 10^{-5}$ g tungsten/cm^2/day[a][68]	11 d[b]	
WO$_3$, aggregated 36,2 μm in artificial lung alveolar macrophage phagolysosomal fluid (pH 4,5)	$9,8 \pm 2,9 \times 10^{-9}$ g tungsten/ cm^2/day[a][68]	9 893 ± 2 549[b]	
Talc, 1 micron particle	$1,4 \times 10^{-11}$ mol Si/m^2/s[b][50]		8 years
Chrysotile, 1 μm fibres pH 2 to 6 at 37 °C	$5,9 \times 10^{-10}$ mol Si/m^2/s[b][153]		9 months to 19 months, depending on diameter
Olivine, 1 micron particle	$7,6 \times 10^{-11}$ mol Si/m^2/s[b][50]		4,8 years
Quartz, 1 micron particle	$1,4 \times 10^{-13}$ mol Si/m^2/s[b][50]		5 000 years
Nanoparticles			
Amorphous silica nanoparticles	$2,57 \times 10^{-12}$ mol Si/m^2/s[159]		2 years[98]
Citrate stabilized Ag 4,8 nm in deionised water, at 0,2 mg/L total silver	0,53/day[c][46]	1,3 d (31,4 h)[98]	
Citrate stabilized Ag 4,8 nm in deionised water, at 2 mg/L total silver	0,023/day[c][46]	30 d (723 h)[98]	
TiO$_2$ 1 nm to 24,4 nm Industrial, In aqueous NaCl solutions at temperatures of 25 and 37 °C - pH ranging between 3,0 and 3,3.	$3,3 \times 10^{-2}$/h[c][160]	21 h[98]	
[a] Normalized zero order rate constant.			
[b] From the shrinking sphere model.			
[c] Non-normalized first order rate constant.			

12 Examples of micrometer mineral particles and fibres where biodurability was assessed using *in vitro* acellular systems

12.1 Glass and asbestos fibres

Dissolution rate constants of glass fibres in Gamble's solution were found to vary from 1 ng/cm^2/h to 50 000 ng/cm^2/h where the experimental conditions are shown to have an impact on dissolution[16]. Similar dissolution studies were also conducted for asbestos fibres and other siliceous fibres[59].

12.2 Silicon dioxide (SiO$_2$)

The solubility of 5 μm to 10 μm crystalline SiO$_2$ as a function of fluid pH, particle size, and SiO$_2$ concentration in Gamble's solution was assessed. The results have indicated that the solubility of SiO$_2$ increased significantly with higher pH, smaller particle size, and mass where smaller particle size was found to be the most important variable for silica solubility in experimental conditions[161].

12.3 Talc

Dissolution rates of a well-characterized sample of powdered talc, a hydrous magnesium silicate mineral with a chemical composition of $Mg_3Si_4O_{10}(OH)_2$, were measured in solvents that mimic fluids found in the human lung. Using the shrinking sphere model, it was found that the dissolution rate constant at 37 °C, determined by measuring the silicon release rate per unit surface area of talc in a mixed-flow reactor system, is 1,4 (±1,0) × 10^{-11} mol $Si/m^2/s$. It was found that the dissolution rate of talc was higher than quartz, but slower than chrysotile and olivine[158].

12.4 Tungsten oxide

The dissolution of tungsten trioxide (WO_3) and tungsten blue oxides (TBOs) containing fibre-shaped tungsten sub-oxide particles of respirable or thoracic size, was assessed using artificial airway SUF and macrophage PSF. The dissolution rates of tungsten compounds were found to be one to four orders of magnitude slower in PSF compared to SUF. In SUF, fibre-containing $WO_{2,66}$ and $WO_{2,51}$ dissolved more slowly than tungsten metal or WO_3. In PSF, all three fibre-containing TBOs dissolved more slowly than tungsten metal. It was concluded that the existing pulmonary toxicological information on tungsten compounds indicates potential for pulmonary irritation and possibly fibrosis[68].

12.5 Beryllium

Dissolution rates of well-characterized samples of process emission dusts and industrial finished product powders from beryllium mining[162][163] and primary production and ceramics machining[164][165][166][167] facilities were measured at 37 °C. Using a static dissolution technique, it was observed that the beryllium dissolution rates differed widely, with range 10^{-5} $g/cm^2/d$ to 10^{-10} $g/cm^2/d$, depending on the chemical form of material (metal, oxide, hydroxide, alloy, salt, silicate) and pH of the simulated lung fluid. In variations of simulated lung airway fluid (Gamble's Solution, pH 7,4), the beryllium release rate per unit surface area of a material was generally lower than the release rate in simulated phagolysosomal fluid (pH 4,5) for the same material. Release of beryllium from multiple chemical constituent particles such as silicate ore materials and ore processing dusts was influenced by the co-dissolution of silica and aluminium[162][163].

13 Examples of nanomaterials where biodurability was assessed using *in vitro* acellular systems

13.1 SWCNTs and MWCNTs

Biodegradability of carbon nanotubes was first demonstrated when SWCNTs, cleaned of metal contaminants via oxidative acidic treatment, which also induces the formation of carboxylic acid groups, were incubated 12 weeks with horseradish peroxidase (HRP) and hydrogen peroxide, a gradual degradation of the SWCNTs, could be observed. The suggestion was that this process could aid in the biodegradability of SWCNT, influencing their biopersistence in the environment and their pathogenic potential[31]. Later, using phagolysosomal simulant fluid *in vitro* to show length reduction of carboxylic acid functionalized SWCNTs over a period of 90 days, the carboxylic oxidation was found to introduce damage in the carbon nanotubes in the form of active sites that provided further oxidative degradation by the simulant fluids[168] and thus supporting the previous findings by Allen et al.[31]. Similar biodegradation of SWCNT in phagolysosomal fluid containing oxidative enzymes of inflammatory cells could also be shown by the previous two investigators[169] where it was concluded that the extent to which carbon nanotubes are biodegraded can be a major determinant of the scale and severity of the associated inflammatory responses in exposed individuals. The most recent study concerning the biodurability of carbon nanotubes was conducted over 24 weeks incubation of SWCNTs and other fibres confirming once again the importance of physicochemical properties influencing their biodegradability[170]. Incubation of MWCNTs in similar digestive components containing HRP and hydrogen peroxide, degradation of purified, oxidized, and nitrogen-doped MWNTs were observed with a layer-by-layer degradation mechanism[171].

13.2 Silver nanoparticles (AgNPs)

Using the static dissolution system followed by ultrafiltration, the dissolution rate of citrate-stabilized AgNPs (13,3 nm) was investigated in deionized water. A first-order rate constant (k) of 0,073 4/h for silver ions released from 0,05 mg/L total AgNPs was calculated at 22° C within 6 h[172]. A similar static system followed by ultrafiltration, the dissolution of 4,8 nm could observe a dissolution constant (k) value of 7,6 ug/d/m^2 × 10^{16} ug/d/m^2 and dissolution time to be ranging between 6 d to 125 d depending on the initial concentration of the AgNPs, and on the presence or absence of oxygen, the pH and humic or fulvic acids of the dissolution medium.[46] Using nanosphere lithography (NSL) to fabricate uniform arrays of AgNPs immobilized on glass substrates, the dissolution of AgNP in an air-saturated phosphate buffer (pH 7,0, 25 °C) under variable sodium chloride (NaCl) concentrations was investigated. It was seen that the dissolution rates varied linearly from 0,4 nm/d to 2,2 nm/d over the 10 mM to 550 mM NaCl concentration range tested and therefore it was concluded that the presence of NaCl can play an important role in AgNP fate in saline waters and biological media[139].

The dissolution of AgNPs in simulated gastric fluid was also investigated[80][81][82][83]. Although these and other publications have investigated the dissolution of silver ions from AgNPs, no attempts were made to calculate the dissolution rate constants or to assess the life time disappearance of the investigated AgNPs[80][83][173][174].

There are many factors that affect the dissolution of AgNPs using different environmental media. These include pH, dissolved oxygen[46][80], the ionic strength or hardness of the dissolution liquid, exposure to sunlight[175][176] and the presence of strong complexing ligands for silver where the formation of these complexes with silver ions is more thermodynamically favoured[177][178]. The capping agent might prevent the dissolution of Ag$^+$ [178], or it might not prevent the dissolution as in the study of Khan, et al.[179], where the citrate-coated AgNPs still released Ag$^+$ ions. This could be attributed to the fact that in high ionic strength solutions, coatings can become unstable and dissolve, leaving the NPs unprotected[180]. The coatings might not prevent dissolution but the kinetics of the dissolution could be affected[173].

Using the newly emergent spICP-MS methodology, it was possible to examine the dissolution of AgNPs at environmentally relevant concentrations and to quantitatively evaluate the resultant dissolution rates in a variety of aquatic matrices where the dissolution was measured primarily as a decrease in particle diameter over time with simultaneous direct measurement of released Ag$^+$ (aq)[142][143][144][145][146][147]. Once again, no dissolution kinetics or dissolution rates were reported.

13.3 Titanium dioxide (TiO$_2$)

Titanium dioxide exists in amorphous and in three crystalline forms, i.e. anatase, rutile, and brookite, each of which exhibits different physical properties and photochemical reactivity. Using the static dissolution system followed by centrifugation, the dissolution of TiO$_2$ nanoparticles (60 % crystalline anatase and 40 % amorphous phase) were investigated at different pH ranges and also in the presence of sodium chloride over a period of 3 000 h. Although the thermodynamic equilibrium constants were presented, no dissolution rate constants or life time disappearance were assessed[160][181]. A similar dissolution study was also conducted by others once again with no attempts to determine the dissolution kinetics, dissolution rate constants or halftime of the nanoparticles studied[182]. Most recently, the contrast in dissolution rate constants, half-lives, and static dissolution (solubility) has been investigated at gastric pH (1,5) and neutral lung pH for nano-anatase and nano-rutile and their bulk analogues[183].

13.4 Zinc oxide (ZnO)

Using the static dissolution system followed by filtration, the dissolution of ZnO nanoparticles was studied in pure water as well as in environmental stimulant moderately hard water and also in two culture media namely Dulbecco's Modified Eagle's Medium (DMEM) and Roswell Park Memorial Institute (RPMI)-1640 medium. Once again, no dissolution rate constants were calculated[145], but the importance of size, pH, ionic strength, and adsorption of humic acid in this dissolution was confirmed[101][184].

Most recently, the contrast in dissolution rate constants, halflives, and static dissolution (solubility) has been investigated at gastric pH (1,5) and neutral lung pH for nano zinc oxide and their bulk analogues[183].

14 Biodurability of ligands

14.1 General

Ligands play a dual role in the dissolution process, as protective role and thus decreasing dissolution or enhancing dissolution through a ligand-promoted process.

Functionalization of nanoparticles and fibres with ligands carrying different functional groups is achieved either via *in situ* functionalization through the introduction of these groups during the synthesis of nanoparticles or via post synthesis functionalization through grafting of certain organic groups on the preformed nanoparticles. Once inside the cell, the biodegradability of coating material and or ligands with functional groups (biodefuntionalization) may occur. Wide variety of engineered nanomaterial intentional surface functionalizations and unintentional surface coatings protect but also promote the dissolution of nanomaterials depending on the strength of ligand binding, composition, density and also on their biodurability in biological surroundings. Hence, the distinction should be made between the biodurability of the core nanoparticles and those of the ligands/coating material.

14.2 Examples of ligands attached to particles where biodurability has been assessed

An example of defunctionalization through enzymatic/radical in origin could be confirmed for intravenously administrated PEGylated SWCNTs (PEG-SWCNTs) in liver of mice over time where organ-dependent biodegradation of the ligands were demonstrated as PEG-SWCNTs were shown to be slowly defunctionalized in liver, while they were very stable against biotransformation in spleen for more than eight weeks[185].

Defunctionalisation of nanomaterials could also be demonstrated *in vitro*. For example, dissociation of thiolate ligands from cadmium chalcogenide nanocrystals was observed to occur at low pHs[47] resulting in concerns that low pH of the gastric fluid could also cause their degradation. Subsequently, the low pH of the gastric fluid could indeed be shown to cause degradation of PEG surface coating of QDs[70][84] as well as of the unintentional protein coating (corona) of nanomaterials[186]. On the other hand, increase in pH as well as the presence of ligands such as humic and fulvic acids[46] or sodium dodecyl sulfate (SDS) and Tween could inhibit the dissolution of the AgNPs[100] could inhibit the dissolution of AgNPs in natural waters. Similar degradation of the ligands and other coating materials and thus biomodification of nanomaterials were also seen with environmental samples. For example, the digestion of the lysophosphatidylcholine coating on single-walled carbon nanotube by *Daphnia magna* was reported providing evidence of biomodification of a carbon-based nanomaterial by an aquatic organism[187].

14.3 Methodologies to assess the biodurability of the attached ligands

14.3.1 General

Gel permeation chromatography (GPC), matrix-assisted laser desorption/ionization time-of-flight mass spectrometry (MALDI-TOF-MS) and attenuated total reflectance-Fourier transform infrared (ATR-FTIR) spectroscopy are usually employed to assess the surface ligands attached to nanomaterials and liquid chromatography-mass spectroscopy-mass spectroscopy (LC-MS/MS) is useful for characterizing proteins that have adsorbed to the surface of nanomaterials.

14.3.2 Gel permeation chromatography (GPC)

Gel permeation chromatography (GPC) is a form of liquid chromatography, where both solid stationary and liquid mobile phases are used. Using GPC, it was possible to assess the biodegardability of polyethylene glycol, polypeptoids and poly(2-oxazoline)s that are used as ligands for nanoparticles[188].

14.3.3 Matrix-assisted laser desorption ionization mass spectrometer (MALDI-MS)

MALDI-TOF-MS is a versatile method to analyse macromolecules from biological origin, the general principle of which revolves around the rapid photo-volatilization of a sample embedded in a UV-absorbing matrix followed by time-of-flight mass spectrum analysis[189]. Using this advanced methodology[190][191], the stability of monolayers on quantum dots in live cells[192] and also gold nanoparticles[193] was investigated where the presence of intracellular biothiols such as glutathione or cysteine were suggested to degrade the monolayers on these nanoparticles and thus drastically alter their colloidal stability and functionality.

14.3.4 Attenuated total reflectance-Fourier transform infrared spectroscopy (ATR-FTIR)

ATR-FTIR spectroscopy is usually employed to assess the surface ligands attached to nanoparticles[194][195][196]. This methodology can also be implemented to assess the changes and hence their biodurability *in vitro* in different biological and environmental media.

14.3.5 Liquid chromatography coupled with mass spectrometry (LC-MS/MS)

Liquid chromatography coupled with mass spectrometry (LC-MS/MS) is a powerful analytical technique that combines the resolving power of liquid chromatography with the detection specificity of mass spectrometry where analytes are detected directly from molecular characteristics as molecular mass and molecular disintegration patterns in mass spectrometric method. The latter does not directly determine mass but, determines the mass of a molecule by measuring the m/z ratios of its ion. MS/MS is the combination of two mass analyzers in one mass spec instrument the first of which filters for the precursor ion followed by a fragmentation of the precursor ion and the second then filters for the product ions, generated by the fragmentation usually using in a triple quadrupole (QQQ) or a quadrupole time-of-flight (QTOF). Using this technique, it was possible to investigate the protein-based ligands around the sulfonated polystyrene and silica[197], as well gold, nanoparticles[198].

15 Relationship with relevant international documents

15.1 Simulated sweat

— ASTM D2322-00

— ASTM D7019-05

— ASTM D7020-05

— ASTM D7021-05

— ASTM D7268-06

— ASTM D3730-10

— ASTM F619-03

— AATCC Test Method 15-2002

— AATCC Test Method 125-2004

— ISO 105-E04:2013

— ISO 3160-2

— ISO 7620:2005

— ISO 9022-12:1994

— ISO 11640:1993

— ISO 11641:1993

— ISO 12870:2004

— ISO 17700:2004

— ISO 22652:2002

— ISO 24348:2007

— DIN 53160-2010

— EN 1811

— EN 12801:2000

— EN 13516:2001

— EN 16128:2011

— Oeko-Tex® Standard 200, 3

— Oeko-Tex® Standard 200, 10

15.2 Simulated sebum

— ASTM D4008-95

— ASTM D4265-98

— ASTM D5343-06

15.3 Simulated lung fluids

No standard as yet exists for simulated lung fluid.

15.4 Simulated digestive system fluids

— ASTM D5517-03 A

— BS EN 71-9:2005+A1:2007

— BS EN 15517:2008

— DIN 53160-1:2010

— BS EN 12868:1999

16 Assessing the validity of assay/test systems

Cell-free *in vitro* dissolution test systems have been used extensively for over 40 years. During that time, several investigators have compared results obtained from various dissolution test systems to *in vivo* data. Considerably more data is available for micrometre particles and fibres as there is a longer history of testing in the literature. One of the earliest studies was by Kanapilly et al[60] who evaluated the dissolution of various radiolabelled particles in different cell-free *in vitro* test systems using artificial airway epithelial airway lining fluid and compared results to *in vivo* studies using beagle dogs. The authors reported good agreement between *in vitro* and *in vivo* results for zirconium oxalate and strontium-90 (^{90}Sr)-fused clay particles. For example, using ^{90}Sr-fused clay particles the calculated chemical dissolution rate constants for the cell-free test systems were 3,1 g/cm^2/d × 10^{-8} g/cm^2/d (static system) and 3,3 g/cm^2/d × 10^{-8} g/cm^2/d (continuous flow system) which agreed with the value of 3,4 g/cm^2/d × 10^{-8} g/cm^2/d determined *in vivo*. In another pulmonary study[199], it was reported

there was good agreement between dissolution rates of uranium tetrafluoride observed in a static system with Gamble's solution containing superoxide ion compared to *in vivo* data from inhalation by rats and humans. In a study involving dermal exposures[200], experts evaluated the dissolution of cobalt from cemented tungsten carbide "hard metal" discs using artificial sweat (pH 6,5) and patch tested cobalt-sensitized volunteers with the same discs. All discs released cobalt in artificial sweat and all discs elicited positive skin reactions. The authors concluded that the concentration of cobalt released from the discs in artificial sweat was high enough to elicit allergic contact dermatitis in cobalt-sensitized patients.

With regard to nanoscale materials, in a series of independent studies using the same ultrafine (200 nm) beryllium oxide particles, chemical dissolution rate constants were determined using a static dissolution test system with artificial PSF (pH 4,5)[67], *in vitro* phagolysosomal dissolution by J774A.1 murine monocyte-macrophage cells[201], and *in vivo* using beagle dogs[202]. The calculated chemical dissolution rate constant in PSF (1,2 g/cm^2/d × 10^{-8} g/cm^2/d) was within a factor of two of the rate constant determined *in vitro* using the J774A.1 cell line (2,3 10^{-8} g/cm^2/d) and showed good agreement to the rate constant determined *in vivo* (0,7 g/cm^2/d × 10^{-8} g/cm^2/d). More recently[203], Jeong et al. evaluated dissolution of indium oxide nanoparticles and CuONPs in an artificial lysosomal fluid (pH 5,5) at 1 and 28 d and measured particle toxicity *in vivo* using rats on several days up to 28 d post-exposure. Dissolution of CuONPs was very rapid, with over 97 % dissolving by day one and the remaining 3 % dissolving thereafter. This dissolution data tracked with the *in vivo* data for CuONPs that showed severe neutrophilic inflammation on day one but the symptoms were completely resolved by day 14; no pulmonary alveolar proteinosis (PAP) was observed on day 28. In contrast, the dissolution of indium oxide nanoparticles was slower and progressive with 0,6 % of the indium dissolved in the artificial lysosomal fluid on day one and 5,5 % on day 28. These dissolution data were consistent with observed *in vivo* results that showed progressively worsening neutrophilic inflammation from day one to day 28 and severe PAP on day 28.

While the above mentioned studies do not validate cell-free *in vitro* dissolution test systems in the strict sense, they do suggest that these tests are a starting place to produce biologically relevant data that will aid risk assessment of nanomaterials.

As stated by Misra et al.[29], the way forward to measure dissolution of NPs should entail (i) developing standard protocol(s) to measure dissolution of NPs addressing the technical difficulties of separating NPs from ionic species, (ii) better understanding of the complex role of physicochemical properties on dissolution and (iii) accounting for interaction of NPs with the exposure media and its effect on dissolution.

17 Biological relevance of the dissolution assay

It is said that dissolution might be among the critical steps for some nanomaterials in determining fate in the environment and within the body and that dissolution over time could significantly enhance clearance of nanomaterials[204]. The observations that the similarities in amenability of particles to chemical dissolution *in vitro* and *in vivo* suggest that their susceptibility to dissolution *in vitro* may be a useful predictor to their biodurability *in vivo*[99].

As for pathogenicity, evidence indicated that highly soluble fibrous particles do not exhibit fibrotic or carcinogenic potential in animal studies. *In vitro* dissolution studies are therefore proposed to provide a rapid and more controlled alternative to classic long-term toxicity testing in animals and could provide useful information when performed as companion experiments with *in vivo* studies if conditions of exposure and test agent can be made similar. Although uncertainties exist about the specific physiological processes that occur in the lung, results from *in vitro* assays can provide some insight into the chemical reactions that influence particle and fibre dissolution. As such, both *in vitro* and *in vivo* dissolution studies on particles have been used to assess their biopersistence and hence as a measure to predict their potential chronic effects[204].

18 Use of biodurability tests in risk assessment and its limitations

A compilation of tests used and methodologies described in the literature to determine the dissolution and biodegradation of nanomaterials as indicators of biodurability is an important contribution to the need for rapid hazard assessment of nanomaterials and augments the ability of *in vitro* assay systems in the identification of potential adverse effects of nanomaterials[29]. We know from studies of micrometre-scale particles that material dissolution is an important factor in toxicokinetic or physiologically-based pharmacokinetic (PBPK) modelling to estimate the target tissue dose associated with an adverse response. In studies by Schroeter et al.[205][206] and Taylor et al.[207], dissolution of micrometre-scale particles was a component of clearance kinetics and dose estimation for manganese accumulation in the brain which is critical for translation of animal data to human health risk assessment of neurotoxicity. With regard to human risk assessment of nanomaterials, dissolution and biodurability are recognized as important components of assessments[208][209] and play a critical role in the development of occupational exposure limits for materials such as AgNPs (NIOSH, unpublished data) and in safety-by-design (prevention-through-design) efforts[210]. Ecological (non-occupational human, animal, and environmental) risk assessments of nanomaterials also utilize dissolution data. In studies of a cerium oxide nanomaterial used as a fuel additive[211], it is reported that dissolution of combusted cerium in simulated soft water was a factor of one hundred higher compared to the catalyst form. Released cerium was below levels expected to represent a risk to aquatic organisms and was predicted to interact with soil in the environment thereby reducing toxicological risk to soil organisms.

Annex A
(informative)

Tables of relevant information

Table A.1 — Simulated lung extracellular fluid composition in various studies[59][158][[212][213]

Component	Concentration (mg/L)			
	Reference [213]	Reference [212]	Reference [158]	Reference [59]
$MgCl_2 \cdot 6H_2O$	212	212	212	212
NaCl	6 415	6 415	6 400	6 415
$CaCl_2 \cdot 2H_2O$	255	193 ($CaCl_2$)	255	318 ($CaCl_2$ to $4H_2O$)
Na_2SO_4	79	79	179 $Na_2SO_4.10H_2O$	179 $Na_2SO_4 \cdot 10H_2O$
Na_2HPO_4	148	358 $Na_2HPO_4 \cdot 12H_2O$	148	148
$NaHCO_3$	2 703	2 703	2 700	2 703
$C_4H_4Na_2O_6$ (anhydrous) (Sodium tartrate)	199	180 ($C_4H_8Na_2O_8$ (dihydrate)	180 ($C_4H_8Na_2O_8$ (dihydrate)	180 ($C_4H_8Na_2O_8$ (dihydrate)
$HOC(COONa)(CH_2COONa)_2 \cdot 2H_2O$ Trisodium citrate dihydrate	180	153	153	186 $HOC(COONa)(CH_2COONa)_2 \cdot 5H_2O$ Trisodium citrate pentahydrate
$C_3H_5NaO_3$ Sodium lactate	175	175	290 (60 % w/w)	175
$C_3H_3NaO_3$ Sodium pyruvate	172	172	172	172
NH_2CH_2COOH Glycine	118	118	118	118
CH_2O (Formaldehyde) was added in order to prevent the growth of algae or bacteria		1 mI/I		1 mI/I
ovalbumin (when used)			445	

Table A.2 — Phagolysosomal simulant fluid (PSF) compositions[67][69][168]

Component	Concentration (mg/L)
Concentration	References [67][69][168]
Na_2HPO_4 (Sodium phosphate dibasic anhydrous)	142
NaCl (Sodium chloride)	6 650
Na_2SO_4 (Sodium sulfate, anhydrous)	71
$CaCl_2.2H_2O$ (Calcium chloride dehydrate)	29
NH_2CH_2COOH (Glycine)	450
$C_8H_5O_4K$ (Potassium hydrogen phthalate)	4 084,6

Table A.3 — Simulated saliva (SS) compositions[57]

Composition	SS 1 (g/L)	SS 2 (g/L)	SS 3 (g/L)	SS 4 (g/L)	SS 5 (g/L)
KCl (Potassium chloride)	0,720	0,720	—	0,149	
$CaCl_2.2H_2O$ (Calcium chloride dehydrate)	0,220	0,220	0,228	—	
NaCl (Sodium chloride)	0,600	0,600	1,017	0,117	8,00
KH_2PO_4 (Potassium phosphate monobasic)	0,680	0,680	—	—	0,19
Na_2HPO_4 (Sodium phosphate dibasic)	0,866 ($Na_2HPO_4 \cdot 12.H_2O$)	0,866 ($Na_2HPO_4 \cdot 12.H_2O$)	0,204 ($Na_2HPO_4 \cdot 7.H_2O$)	—	2,38
$KHCO_3$ (Potassium bicarbonate)	1,500	1,500	—	—	
KSCN (Potassium thiocyanate)	0,060	0,060	—	—	
$C_6H_8O_7$ (Citric acid)	0,030	0,030	—	—	
$MgCl_2.6H_2O$ (Magnesium chloride hexahydrate)	—	—	0,061	—	
$K_2CO_3 \cdot 2H_2O$ (Potassium carbonate hemihydrates)	—	—	0,603	—	
$NaH_2PO_4 \cdot H_2O$ (Sodium phosphate monobasic monohydrate)	—	—	0,273	—	
$NaHCO_3$ (Sodium bicarbonate)	—	—	—	2 100	
Submaxillary mucin	—	—	1 000	—	
α-Amylase	—	—	2 000	2 000	
Mucin gastric	—	—	—	1 000	
pH	6,5	7,4	—	—	6,8

Table A.4 — Simulated gastrointestinal fluids compositions[70]

Component	Concentration (g/L) gastric juice	Concentration (g/L) Intestinal fluid
NaCl (Sodium chloride)	0,05 M (2,922 g/L)	
KCl (Potassium chloride)	0,094 M (7,007 822 2 g/L)	0,004 M (0,298 g/L)
K_2HPO_4 (Potassium hydrogen phosphate)	0,001 4 M (0,243 88 g/L)	
$CaCl_2$ (Calcium chloride)		0,004 5 M (0,499 g/L)
$MgCl_2$ (Magnesium chloride)		0,002 M (0,190 g/L)
NH_2CONH_2 Urea		0,005 M (0,300 g/L)
Pepsin	1 mg/ml	
Mucin	3 mg/ml	
Bile salts		9 mg/ml
Pancreatin		9 mg/ml
O_2 (Oxygen)	0,000 22 M	0,000 22 M
E_H (Hydrogen electrode potential)	+1,02 V	+0,69 V
pH	Reference [2]	References [7] and [5]

Table A.5 — Simulated sweat (SSW) compositions[57]

Salt	SSW(3)[a]	SSW(60)[a]	SSW(120)[a]	SSW(240)[a]
NaCl (Sodium chloride)	2,92	5,49	5,49	5,49
$CaCl_2$ (Calcium chloride)	0,166	3,32	6,64	13,28
$MgSO_4$ (Magnesium sulfate)	0,12	0,24	0,24	0,24
KH_2PO_4 (Potassium phosphate monobasic)	1,02	1,36	1,36	1,36
pH	5,4	4,5	4,5	4,5
[a] The numbers in parentheses indicate milliequivalents of calcium ions.				

Table A.6 — Simulated freshwater compositions: Preparation of synthetic freshwater using reagent grade chemicals[a][51][214]

Water type	Reagent added (mg/L)[b]				Approximate final water quality		
	$NaHCO_3$	$CaSO_4·2H_2O$	MgSO4	KCl	pH[c]	Hardness[d]	Alkalinity[d]
Very soft	12,0	7,5	7,5	0,5	6,4 to 6,8	10 to 13	10 to 13
Soft	48,0	30,0	30,0	2,0	7,2 to p7,6	40 to 48	30 to 35
Moderately hard	96,0	60,0	60,0	4,0	7,4 to 7,8	80 to 100	60 to 70
Hard	192,0	120,0	120,0	8,0	7,6 to 8,0	160 to 180	110 to 120
Very hard	384,0	240,0	240,0	16,0	8,0 to 8,4	280 to 320	225 to 245
[a] Taken in part from Marking and Dawson (1973)[213].							
[b] Add reagent grade chemicals to deionized water.							
[c] Approximate equilibrium pH after 24 h of aeration.							
[d] Expressed as mg $CaCO_3$/L.							

Table A.7 — GP2[a] Simulated seawater composition[51][96]

Compound	Concentration (g/L)	Amount (g) required for 20 L
NaCl (Sodium chloride)	21,03	420,6
Na_2SO_4 (Sodium sulfate, anhydrous)	3,52	70,4
KCl (Potassium chloride)	0,61	12,2
KBr (Potassium bromide)	0,088	1,76
$Na_2B_4O_7.10\ H_2O$ (Borax)	0,034	0,68
$MgCl_2.6H_2O$ (Magnesium chloride hexahydrate)	9,50	190,0
$CaCl_2.2H_2O$ (Calcium chloride dehydrate)	1,32	26,4
$SrCl_2.6H_2O$ (Strontium Chloride Hexahydrate)	0,02	0,400
$NaHCO_3$ (Sodium bicarbonate))	0,17	3,40
[a] GP stands for general purpose.		

Table A.8 — Simulated Estuarine Water composition[216]

Element	Concentration (µg/L)
Cr (Chromium)	0,139
Mn (Manganese)	13,1
Fe (Iron)	2,08
Co (Cobalt)	0,046
Ni (Nickel)	0,743
Cu (Cupper)	1,76
Zn (Zinc)	0,86
As (Arsenic)	0,765
Cd (Cadmium)	0,018
Pb (Lead)	0,028

Bibliography

[1] OBERDORSTER G.F.J. Correlation between particle size, in vivo particle persistence, and lung injury. *Environ. Health Perspect.* 1994, **102** () pp. 173–179

[2] LIPPMANN M., YEATES D.B., ALBERT R.E. Deposition, retention, and clearance of inhaled particles. *Br. J. Ind. Med.* 1980, **37** pp. 337–362

[3] BROWN DM, KINLOCH JA, BANGERT U, WINDLE AH M. WD, Walker GS, Scotchford CA., Donaldson K & Stone V. An in vitro study of the potential of carbon nanotubes and nanofibers to induce inflammatory mediators and frustrated phagocytosis. *Carbon.* 2007, **45** pp. 1743–1756

[4] GEISER M., CASAULTA M., KUPFERSCHMID B., SCHULZ H., SEMMLER-BEHNKE M., KREYLING W. The role of macrophages in the clearance of inhaled ultrafine titanium dioxide particles. *Am. J. Respir. Cell Mol. Biol.* 2008, **38** pp. 371–376

[5] Canada (2000) Canadian Environmental Protection Act, 1999: Persistence and Bioaccumulation Regulations, P.C. 2000-348, 23 March, 2000, SOR/2000-107, Canada

[6] Canada (2013) Environment Health Canada Screening Assessment for the Challenge CAS RN 14808-60-7, 14464-46-1 In *Toxicol Lett*

[7] CHAPPELL M.A., GEORGE A.J., DONTSOVA K.M., PORTER B.E., PRICE C.L., ZHOU P. Surfactive stabilization of multi-walled carbon nanotube dispersions with dissolved humic substances. *Environ. Pollut.* 2009, **157** pp. 1081–1087

[8] PAN J.F., BUFFET P.E., POIRIER L., AMIARD-TRIQUET C., GILLILAND D., JOUBERT Y. Size dependent bioaccumulation and ecotoxicity of gold nanoparticles in an endobenthic invertebrate: the Tellinid clam *Scrobicularia plana. Environ. Pollut.* 2012, **168** pp. 37–43

[9] BUFFET P.E., AMIARD-TRIQUET C., DYBOWSKA A., RISSO-DE FAVERNEY C., GUIBBOLINI M., VALSAMI-JONES E. Fate of isotopically labeled zinc oxide nanoparticles in sediment and effects on two endobenthic species, the clam *Scrobicularia plana* and the ragworm *Hediste diversicolor. Ecotoxicol. Environ. Saf.* 2012, **84** pp. 191–198

[10] CROTEAU M.N., MISRA S.K., LUOMA S.N., VALSAMI-JONES E. Bioaccumulation and toxicity of CuO nanoparticles by a freshwater invertebrate after waterborne and dietborne exposures. *Environ. Sci. Technol.* 2014, **48** pp. 10929–10937

[11] RAMSKOV T., SELCK H., BANTA G., MISRA S.K., BERHANU D., VALSAMI-JONES E. Bioaccumulation and effects of different-shaped copper oxide nanoparticles in the deposit-feeding snail Potamopyrgus antipodarum. *Environ. Toxicol. Chem.* 2014, **33** pp. 1976–1987

[12] ZHU X.S., CHANG Y., CHEN Y.S. Toxicity and bioaccumulation of TiO_2 nanoparticle aggregates in *Daphnia magna. Chemosphere.* 2010, **78** pp. 209–215

[13] GARCIA-ALONSO J., RODRIGUEZ-SANCHEZ N., MISRA S.K., VALSAMI-JONES E., CROTEAU M.N., LUOMA S.N. Toxicity and accumulation of silver nanoparticles during development of the marine polychaete Platynereis dumerilii. *Sci. Total Environ.* 2014, **476-477** pp. 688–695

[14] DAVIS J.M. The role of clearance and dissolution in determining the durability or biopersistence of mineral fibers. *Environ. Health Perspect.* 1994, **102** (Suppl 5) pp. 113–117

[15] MAXIM L.D., HADLEY J.G., POTTER R.M., NIEBO R. The role of fiber durability/biopersistence of silica-based synthetic vitreous fibers and their influence on toxicology. *Regul. Toxicol. Pharmacol.* 2006, **46** pp. 42–62

[16] Mattson S.M. Glass fiber dissolution in simulated lung fluid and measures needed to improve consistency and correspondence to in vivo dissolution. *Environ. Health Perspect.* 1994, **102** () pp. 87–90

[17] Potter R.M. Method for determination of *in-vitro* fiber dissolution rate by direct optical measurement of diameter decrease. *Glastechnische Berichte Glass Science and Technology*. 2000, **73** pp. 46–55

[18] Sebastian K, Fellman J, Potter R, Bauer J, Searl A, de Meringo A, Maquin B, de Reydellet A, Jubb G, Moore M, Preininger R, Zoitos B P. B, Steenberg T, Madsen AL & Guldberg M. EURIMA test guideline: *In vitro* acellular dissolution of man-made vitrous silicate fibres. *Glass Science Technology*. 2002, **75** pp. 263–270

[19] Holmes A., & Morgan A. Leaching of constituents of chrysotile asbestos *in vivo. Nature*. 1967, **215** pp. 441–442

[20] Langer A.M., Rubin I.B., Selikoff I.J., Pooley F.D. Chemical characterization of uncoated asbestos fibers from the lungs of asbestos workers by electron microprobe analysis. *J. Histochem. Cytochem.* 1972, **20** pp. 735–740

[21] Jaurand M.C., Bignon J., Sebastien P., Goni J. Leaching of chrysotile asbestos in human lungs. Correlation with *in vitro* studies using rabbit alveolar macrophages. Environ. Res. 1977, **14** pp. 245–254

[22] Morgan A., Holmes A., Davison W. Clearance of sized glass fibres from the rat lung and their solubility in vivo. *Ann. Occup. Hyg.* 1982, **25** pp. 317–331

[23] Bernstein D., Castranova V., Donaldson K., Fubini B., Hadley J., Hesterberg T. Testing of fibrous particles: short-term assays and strategies. *Inhal. Toxicol.* 2005, **17** pp. 497–537

[24] Jaurand M.C., Gaudichet A., Halpern S., Bignon J. *In vitro* biodegradation of chrysotile fibres by alveolar macrophages and mesothelial cells in culture: comparison with a pH effect. *Br. J. Ind. Med.* 1984, **41** pp. 389–395

[25] Jaurand M.C. *In vitro* assessment of biopersistence using mammalian cell systems. *Environ. Health Perspect.* 1994, **102** () pp. 55–59

[26] Johnson N.F. Phagosomal pH and glass fiber dissolution in cultured nasal epithelial cells and alveolar macrophages: a preliminary study. *Environ. Health Perspect.* 1994, **102** () pp. 97–102

[27] Nguea H.D., de Reydellet A., Le Faou A., Zaiou M., Rihn B. Macrophage culture as a suitable paradigm for evaluation of synthetic vitreous fibers. *Crit. Rev. Toxicol.* 2008, **38** pp. 675–695

[28] Malkiewicz K, Pettitt M, Dawson KA, Toikka A, Hansson SO, Hukkinen J, Lynch I, Lead JR (2011) Nanomaterials in REACH - evaluation of applicability of existing procedures for chemical safety assessment to nanomaterials. 15 August

[29] Misra S.K., Dybowska A., Berhanu D., Luoma S.N., Valsami-Jones E. The complexity of nanoparticle dissolution and its importance in nanotoxicological studies. *Sci. Total Environ.* 2012, **438** pp. 225–232

[30] Franklin N.M., Rogers N.J., Apte S.C., Batley G.E., Gadd G.E., Casey P.S. Comparative toxicity of nanoparticulate ZnO, bulk ZnO, and $ZnCl_2$ to a freshwater microalga (*Pseudokirchneriella subcapitata*): the importance of particle solubility. *Environ. Sci. Technol.* 2007, **41** pp. 8484–8490

[31] Allen B.L., Kichambare P.D., Gou P., Vlasova I.I., Kapralov A.A., Konduru N. Biodegradation of single-walled carbon nanotubes through enzymatic catalysis. *Nano Lett.* 2008, **8** pp. 3899–3903

[32] Oberdörster G., Oberdörster E., Oberdörster J. Nanotoxicology: an emerging discipline evolving from studies of ultrafine particles. *Environ. Health Perspect.* 2005, **113** pp. 823–839

[33] Zhu M.T., Feng W.Y., Wang Y., Wang B., Wang M., Ouyang H. Particokinetics and extrapulmonary translocation of intratracheally instilled ferric oxide nanoparticles in rats and the potential health risk assessment. *Toxicol. Sci.* 2009, **107** pp. 342–351

[34] Geiser M. Update on macrophage clearance of inhaled micro- and nanoparticles. *J. Aerosol Med. Pulm. Drug Deliv.* 2010, **23** pp. 207–217

[35] He X., Zhang H., Ma Y., Bai W., Zhang Z., Lu K. Lung deposition and extrapulmonary translocation of nano-ceria after intratracheal instillation. *Nanotechnology.* 2010, **21** p. 285103

[36] Petros R.A., & DeSimone J.M. Strategies in the design of nanoparticles for therapeutic applications. *Nat. Rev. Drug Discov.* 2010, **9** pp. 615–627

[37] Ates M., Demir V., Adiguzel R., Arslan Z. Bioaccumulation, Sub-acute Toxicity, and Tissue Distribution of Engineered Titanium Dioxide (TiO) Nanoparticles in Goldfish. *J. Nanomater.* 2013, ••• p. 2013

[38] Brunner T.J., Wick P., Manser P., Spohn P., Grass R.N., Limbach L.K. *In vitro* cytotoxicity of oxide nanoparticles: comparison to asbestos, silica, and the effect of particle solubility. *Environ. Sci. Technol.* 2006, **40** pp. 4374–4381

[39] Oberdörster G. Toxicokinetics and effects of fibrous and nonfibrous particles. *Inhal. Toxicol.* 2002, **14** pp. 29–56

[40] NIOSH. *Current Intelligence Bulletin 62: Asbestos fibres and other elongate mineral particles: State of the science and roadmap for research.* Department of Helath and Human Services. Centers for Disease Control and Prevention National Institute for Occupational Safety and Health, 2011

[41] Light W.G., & Wei E.T. (1977a) Surface charge and asbestos toxicity. *Nature* **265**, pp. 537-539.

[42] Light W.G., & Wei E.T. (1977b) Surface charge and asbestos toxicity. *Environ Re* **13**, pp. 135-145

[43] Vallyathan V., Hanon N., Booth J., Schwegler D., Sepulveda M. 1985) Cytotoxicity of native and surface-modified asbestos. In: Beck EG, Big¬non J, eds. In vitro effects of mineral dusts. Ber¬lin-Heidelberg: Springer-Verlag. NATO ASI Series, Vol. G3, pp. 159–165

[44] Monopoli M.P., Pitek A.S., Lynch I., Dawson K.A. Formation and characterization of the nanoparticle-protein corona. *Methods Mol. Biol.* 2013, **1025** pp. 137–155

[45] Sadauskas E., Danscher G., Stoltenberg M., Vogel U., Larsen A., Wallin H. Protracted elimination of gold nanoparticles from mouse liver. *Nanomedicine (Lond.).* 2009, **5** pp. 162–169

[46] Liu J., & Hurt R.H. Ion Release Kinetics and Particle Persistence in Aqueous Nano-Silver Colloids. *Environ. Sci. Technol.* 2010, **44** pp. 2169–2175

[47] Aldana J., Lavelle N., Wang Y., Peng X. Size-dependent dissociation pH of thiolate ligands from cadmium chalcogenide nanocrystals. *J. Am. Chem. Soc.* 2005, **127** pp. 2496–2504

[48] King-Heiden T.C., Wiecinski P.N., Mangham A.N., Metz K.M., Nesbit D., Pedersen J.A. Quantum dot nanotoxicity assessment using the zebrafish embryo. Environ. Sci. Technol. 2009, **43** pp. 1605–1611

[49] Wiecinski P.N. 2012) Toxicity of intact and weathered nanomaterials to zebrafish. A dissertation submitted in partial fulfillment of the requirements for the degree of Doctor of Philosophy (Molecular and Environmental Toxicology) at the University of Wisconsin-Madison

[50] Jurinski J.B. 1998) Geochemical Investigations of respirable particulate matter. Dissertation submitted to the in partial fulfillment of the requirements for the degree of Doctor of Philosophy in Geological Sciences. June 10., Faculty of the Virginia Polytechnic Institute and State University

[51] EPA (2002) 821/R-02-012: Methods for measuring the acute toxicity of effluents and receiving waters to freshwater and marine organisms

[52] Chinnapongse S.L., MacCuspie R.I., Hackley V.A. Persistence of singly dispersed silver nanoparticles in natural freshwaters, synthetic seawater, and simulated estuarine waters. *Sci. Total Environ.* 2011, **409** pp. 2443–2450

[53] Christensen V.R., Jensen S.L., Guldberg M., Kamstrup O. Effect of chemical composition of man-made vitreous fibers on the rate of dissolution *in vitro* at different pHs. *Environ. Health Perspect.* 1994, **102** () pp. 83–86

[54] Gamble J.L. *Chemical Anatomy, Physiology and Pathology of Extracellular Fluid.* Harvard University Press, Cambridge, MA, 1967

[55] Moss O.R. Simulants of lung interstitial fluid. *Health Phys.* 1979, **36** pp. 447–448

[56] Dennis N.A., Blauer H.M., Kent J.E. Dissolution fractions and half-times of single source yellowcake in simulated lung fluids. *Health Phys.* 1982, **42** pp. 469–477

[57] Marques M.R.C., Loebenberg R., Almukainzi M. Simulated Biological Fluids with Possible Application in Dissolution Testing. *Dissolut. Technol.* 2011, (August) pp. 15–28

[58] Kagan V.E., Kapralov A.A., St Croix C.M., Watkins S.C., Kisin E.R., Kotchey G.P. Lung macrophages "digest" carbon nanotubes using a superoxide/peroxynitrite oxidative pathway. *ACS Nano.* 2014, **8** pp. 5610–5621

[59] Scholze H., & Conradt R. An *in vitro* study of the chemical durability of siliceous fibres. *Ann. Occup. Hyg.* 1987, **31** pp. 683–692

[60] Kanapilly G.M., Raabe O.G., Goh C.H., Chimenti R.A. Measurement of *in vitro* dissolution of aerosol particles for comparison to in vivo dissolution in the lower respiratory tract after inhalation. *Health Phys.* 1973, **24** pp. 497–507

[61] Ansoborlo E., Henge-Napoli M.H., Chazel V., Gibert R., Guilmette R.A. Review and critical analysis of available *in vitro* dissolution tests. *Health Phys.* 1999, **77** pp. 638–645

[62] Nyberg K., Johansson A., Camner P. Intraphagosomal pH in alveolar macrophages studied with fluorescein-labeled amorphous silica particles. *Exp. Lung Res.* 1989a, **15** pp. 49–62

[63] Nyberg K., Johansson U., Rundquist I., Camner P. Estimation of pH in individual alveolar macrophage phagolysosomes. *Exp. Lung Res.* 1989b, **15** pp. 499–510

[64] Kreyling W.G. Intracellular particle dissolution in alveolar macrophages. *Environ. Health Perspect.* 1992, **97** pp. 121–126

[65] Nyberg K., Johansson U., Johansson A., Camner P. Phagolysosomal pH in alveolar macrophages. *Environ. Health Perspect.* 1992, **97** pp. 149–152

[66] Lundborg M., Johard U., Johansson A., Eklund A., Falk R., Kreyling W. Phagolysosomal morphology and dissolution of cobalt oxide particles by human and rabbit alveolar macrophages. *Exp. Lung Res.* 1995, **21** pp. 51–66

[67] Stefaniak A.B., Guilmette R.A., Day G.A., Hoover M.D., Breysse P.N., Scripsick R.C. Characterization of phagolysosomal simulant fluid for study of beryllium aerosol particle dissolution. *Toxicol. In Vitro.* 2005, **19** pp. 123–134

[68] Stefaniak A.B. Persistence of tungsten oxide particle/fiber mixtures in artificial human lung fluids. *Part. Fibre Toxicol.* 2010, **7** p. 38

[69] Russier J., Menard-Moyon C., Venturelli E., Gravel E., Marcolongo G., Meneghetti M. Oxidative biodegradation of single- and multi-walled carbon nanotubes. *Nanoscale.* 2011, **3** pp. 893–896

[70] WIECINSKI P.N., METZ K.M., MANGHAM A.N., JACOBSON K.H., HAMERS R.J., PEDERSEN J.A. Gastrointestinal biodurability of engineered nanomaterials: Development of in vitro assay. *Nanotoxicology.* 2009, **3** pp. 202–214

[71] KALANTZI L., GOUMAS K., KALIORAS V., ABRAHAMSSON B., DRESSMAN J.B., REPPAS C. Characterization of the human upper gastrointestinal contents under conditions simulating bioavailability/bioequivalence studies. *Pharm. Res.* 2006, **23** pp. 165–176

[72] HETRICK E.M., SHIN J.H., PAUL H.S., SCHOENFISCH M.H. Anti-biofilm efficacy of nitric oxide-releasing silica nanoparticles. *Biomaterials.* 2009, **30** pp. 2782–2789

[73] SMITH G., SMITH A.J., SHAW L., SHAW M.J. Artificial saliva substitutes and mineral dissolution. *J. Oral Rehabil.* 2001, **28** pp. 728–731

[74] DUFFÓ G.S., & CASTILLO E.Q. Development of an Artificial Saliva Solution for Studying the Corrosion Behavior of Dental Alloys. *Corrosion.* 2004, **60** pp. 594–602

[75] GOHEL M.C., PARIKH R.K., AGHARA P.Y., NAGORI S.A., DELVADIA R.R., DABHI M.R. Application of simplex lattice design and desirability function for the formulation development of mouth dissolving film of salbutamol sulphate. *Curr. Drug Deliv.* 2009, **6** pp. 486–494

[76] KARTAL A., MARVOLA J., MATHEKA J., PELTONIEMI M., SIVEN M. Computational prediction of local drug effect on carcinogenic acetaldehyde in the mouth based on in vitro/in vivo results of freely soluble L-cysteine. *Drug Dev. Ind. Pharm.* 2010, **36** pp. 715–723

[77] ABZHANOVA D., GODYMCHUK A.Y., GUSEV A.A., KUZNETSOV D.V. Solubility of nickel nanoparticles in simulated body fluids. *Adv. Mat. Res.* 2014, **880** pp. 248–252

[78] MINEKUS M, SMEETS-PEETERS M, BERNALIER A, MAROL-BONNIN S, HAVENAAR R, MARTEAU P, ALRIC M, FONTY G Huis in't Veld JH. A computer-controlled system to simulate conditions of the large intestine with peristaltic mixing, water absorption and absorption of fermentation products. *Appl. Microbiol. Biotechnol.* 1999, **53** pp. 108–114

[79] STEFANIAK A.B., VIRJI M.A., HARVEY C.J., SBARRA D.C., DAY G.A., HOOVER M.D. Influence of artificial gastric juice composition on bioaccessibility of cobalt- and tungsten-containing powders. *Int. J. Hyg. Environ. Health.* 2010b, **213** pp. 107–115

[80] ROGERS K.R., BRADHAM K., TOLAYMAT T., THOMAS D.J., HARTMANN T., MA L. Alterations in physical state of silver nanoparticles exposed to synthetic human stomach fluid. *Sci. Total Environ.* 2012, **420** pp. 334–339

[81] MWILU S.K., EL BADAWY A.M., BRADHAM K., NELSON C., THOMAS D., SCHECKEL K.G. Changes in silver nanoparticles exposed to human synthetic stomach fluid: effects of particle size and surface chemistry. *Sci. Total Environ.* 2013, **447** pp. 90–98

[82] PAL T., SAU T.K., JANA N.R. Reversible Formation and Dissolution of Silver Nanoparticles in Aqueous Surfactant Media. *Langmuir.* 1997, **13** pp. 1481–1485

[83] MAURER E.I., SHARMA M., SCHLAGER J.J., HUSSAIN S.M. Systematic analysis of silver nanoparticle ionic dissolution by tangential flow filtration: toxicological implications. *Nanotoxicology.* 2014, **8** pp. 718–727

[84] WANG L., NAGESHA D.K., SELVARASAH S., DOKMECI M.R., CARRIER R.L. Toxicity of CdSe Nanoparticles in Caco-2 Cell Cultures. *J. Nanobiotechnology.* 2008, **6** p. 11

[85] BLANQUET S., ZEIJDNER E., BEYSSAC E., MEUNIER J.P., DENIS S., HAVENAAR R. A dynamic artificial gastrointestinal system for studying the behavior of orally administered drug dosage forms under various physiological conditions. *Pharm. Res.* 2004, **21** pp. 585–591

[86] AGACHE P. In: *Measuring the Skin: Non-Invasive Investigations, Physiology, Normal Constants.* (AGACHE P., & HUMBERT P. eds.). Springer-Verlag, Germany, 2004, pp. 21–31.

[87] PEDERSEN N.B., FREGERT S., BRODELIUS P., GRUVBERGER B. Release of nickel from silver coins. *Acta Derm. Venereol.* 1974, **54** pp. 231–234

[88] HARVEY C.J., LEBOUF R.F., STEFANIAK A.B. Formulation and stability of a novel artificial human sweat under conditions of storage and use. *Toxicol. In Vitro.* 2010, **24** pp. 1790–1796

[89] SARTORELLI P., CENNI A., MATTEUCCI G., MONTOMOLI L., NOVELLI M.T., PALMI S. Dermal exposure assessment of polycyclic aromatic hydrocarbons: in vitro percutaneous penetration from lubricating oil. *Int. Arch. Occup. Environ. Health.* 1999, **72** pp. 528–532

[90] MOTWANI M.R., RHEIN L.D., ZATZ J.L. Differential scanning calorimetry studies of sebum models. *J. Cosmet. Sci.* 2001, **52** pp. 211–224

[91] WERTZ P.W. Human synthetic sebum formulation and stability under conditions of use and storage. *Int. J. Cosmet. Sci.* 2009, **31** pp. 21–25

[92] STEFANIAK A.B., HARVEY C.J., VIRJI M.A., DAY G.A. Dissolution of cemented carbide powders in artificial sweat: implications for cobalt sensitization and contact dermatitis. *J. Environ. Monit.* 2010a, **12** pp. 1815–1822

[93] STEFANIAK A.B. Dissolution of Materials in Contact with Skin Film Liquids. In: *Handbook of Cosmetic Sciences and Technology*, (BAREL A.O., PAYE M., MAIBACH H.I. eds.). CRC Press, Abingdon, UK, Fourth Edition, 2014, pp. 189–224.

[94] PICCAPIETRA F., SIGG L., BEHRA R. Colloidal stability of carbonate-coated silver nanoparticles in synthetic and natural freshwater. *Environ. Sci. Technol.* 2012, **46** pp. 818–825

[95] SMITH E.J., DAVISON W., HAMILTON-TAYLOR J. Methods for preparing synthetic freshwaters. *Water Res.* 2002, **36** pp. 1286–1296

[96] SPOTTE S., ADAMS G., BUBUCIS P.M. GP2 medium is an artificial seawater for culture or maintenance of marine organisms. *Zoo Biol.* 1984, **3** pp. 229–240

[97] GELABERT A, SIVRY Y, FERRARI R, AKROUT A, CORDIER L, NOWAK S, MENGUY N F. BM. Uncoated and coated ZnO nanoparticle life cycle in synthetic seawater. *Environ. Toxicol. Chem.* 2014, **33** pp. 341–349

[98] UTEMBE W., POTGIETER K., STEFANIAK A.B., GULUMIAN M. Dissolution and biodurability: Important parameters needed for risk assessment of nanomaterials. *Part. Fibre Toxicol.* 2015, **12** p. 11

[99] SEARL A., & BUCHANAN D. (2000) Measurement of the durability of manmade vitreous fibres. Historical Research Report TM/00/03, IOM

[100] LI X., LENHART J.J., WALKER H.W. Aggregation kinetics and dissolution of coated silver nanoparticles. *Langmuir.* 2012, **28** pp. 1095–1104

[101] MUDUNKOTUWA I.A., RUPASINGHE T., WU C.M., GRASSIAN V.H. Dissolution of ZnO nanoparticles at circumneutral pH: a study of size effects in the presence and absence of citric acid. *Langmuir.* 2012, **28** pp. 396–403

[102] SEBASTIEN K., DE MERINGO A., ROUYER E., CHRISTENSEN V.R., GULDBERG M., MATTSON S.M. 1994) *In vitro* acellular tests. Summary report of the second workshop of the International Co-operative Research Programme on Assessment of MMMFs Toxicity. Paris

[103] KLINGHOLZ R., & STEINKOPF B. 1984) *The reactions of MMMF in physiological model fluid and in water.* In: Proceedings of Biological Effects of Man-made Mineral Fibres, Vol 2. Proceedings of a WHO/IARC conference held 20-22 April 1982, in Copenhagen. Copenhagen:World Health Organization, pp. 60-86

[104] LEINEWEBER J.P. Solubility of fibres in vitro and in vivo. In: *Biological Effects of Manmade Mineral Fibres.* World Health Organization, Copenhagen, **Vol. 2**, 1984, pp. 87–101.

[105] Searl A., Buchanan D., Cullen R.T., Jones A.D., Miller B.G., Soutar C.A. Biopersistence and durability of nine mineral fibre types in rat lungs over 12 months. *Ann. Occup. Hyg.* 1999, **43** pp. 143–153

[106] Haase A., Arlinghaus H.F., Tentschert J., Jungnickel H., Graf P., Mantion A. Application of laser postionization secondary neutral mass spectrometry/time-of-flight secondary ion mass spectrometry in nanotoxicology: visualization of nanosilver in human macrophages and cellular responses. *ACS Nano.* 2011, **5** pp. 3059–3068

[107] Hagendorfer H., Kaegi R., Traber J., Mertens S.F., Scherrers R., Ludwig C. Application of an asymmetric flow field flow fractionation multi-detector approach for metallic engineered nanoparticle characterization–prospects and limitations demonstrated on Au nanoparticles. *Anal. Chim. Acta.* 2011, **706** pp. 367–378

[108] Romer I., White T.A., Baalousha M., Chipman K., Viant M.R., Lead J.R. Aggregation and dispersion of silver nanoparticles in exposure media for aquatic toxicity tests. *J. Chromatogr. A.* 2011, **1218** pp. 4226–4233

[109] Wei G.-T., Liu F.-K., Wang C.R.C. Shape Separation of Nanometer Gold Particles by Size-Exclusion Chromatography. *Anal. Chem.* 1999, **71** pp. 2085–2091

[110] Mayo J.T., Lee S.S., Yavuz C.T., Yu W.W., Prakash A., Falknera J.C. A multiplexed separation of iron oxide nanocrystals using variable magnetic fields. *Nanoscale.* 2011, **3** pp. 4560–4563

[111] Messaud F.A., Sanderson R.D., Runyon J.R., Williams S.K.R., Otte T., Pasch H. An overview on field-flow fractionation techniques and their applications in the separation and characterization of polymers. *Prog. Polym. Sci.* 2009, **34** pp. 351–368

[112] Lenshof A., & Laurell T. Continuous separation of cells and particles in microfluidic systems. *Chem. Soc. Rev.* 2010, **39** pp. 203–1217

[113] Engel A., Ploger M., Mulac D., Langer K. Asymmetric flow field-flow fractionation (AF4) for the quantification of nanoparticle release from tablets during dissolution testing. *Int. J. Pharm.* 2014, **461** pp. 137–144

[114] Geiss O., Cascio C., Gilliland D., Franchini F., Barrero-Moreno J. Size and mass determination of silver nanoparticles in an aqueous matrix using asymmetric flow field flow fractionation coupled to inductively coupled plasma-mass spectrometer and ultraviolet-visible detectors. *J. Chromatogr. A.* 2013, **1321** pp. 100–108

[115] Krueger K.M., Al-Somali A.M., Falkner J.C., Colvin V.L. Characterization of nanocrystalline CdSe by size exclusion chromatography. *Anal. Chem.* 2005, **77** pp. 3511–3515

[116] Chekli L., Phuntsho S., Roy M., Shon H.K. Characterisation of Fe-oxide nanoparticles coated with humic acid and Suwannee River natural organic matter. *Sci. Total Environ.* 2013, **461-462** pp. 19–27

[117] Wallace R.M. Concentration and separation of ions by Donnan membrane equilibrium. *Ind. Eng. Chem. Process Des. Dev.* 1967, **6** pp. 423–431

[118] Pyrzynska K. Atomic absorption spectrophotometric determination of gold with preconcentration by Donnan dialysis. *Talanta.* 1994, **41** pp. 381–386

[119] Kennedy A.J., Hull M.S., Bednar A.J., Goss J.D., Gunter J.C., Bouldin J.L. Fractionating nanosilver: importance for determining toxicity to aquatic test organisms. *Environ. Sci. Technol.* 2010, **44** pp. 9571–9577

[120] Hinds W.C. *Aerosol technology: Properties, behaviour, and measurement of airborne particles.* John Wiley & Sons, Inc, New York, Second Edition, 1999, pp. 49.

[121] Levard C., Reinsch B.C., Michel F.M., Oumahi C., Lowry G.V., Brown G.E. Sulfidation processes of PVP-coated silver nanoparticles in aqueous solution: impact on dissolution rate. *Environ. Sci. Technol.* 2011, **45** pp. 5260–5266

[122] Xu M., Li J., Hanagata N., Su H., Chen H., Fujita D. Challenge to assess the toxic contribution of metal cation released from nanomaterials for nanotoxicology–the case of ZnO nanoparticles. *Nanoscale.* 2013, **5** pp. 4763–4769

[123] Chen S., Yao H., Kimura K. Reversible Transference of Au Nanoparticles across the Water and Toluene Interface: A Langmuir Type Adsorption Mechanism. *Langmuir.* 2001, **17** pp. 733–739

[124] Yang J., Lee J.Y., Too H.-P. A general phase transfer protocol for synthesizing alkylamine-stabilized nanoparticles of noble metals. *Anal. Chim. Acta.* 2007, **588** pp. 34–41

[125] Ciesa F., & Plech A. Gold nanoparticle membranes as large-area surface monolayers. *J. Colloid Interface Sci.* 2010, **346** pp. 1–7

[126] Hollamby M.J., Eastoe J., Chemelli A., Glatter O., Rogers S., Heenan R.K. Separation and purification of nanoparticles in a single step. *Langmuir.* 2010, **26** pp. 6989–6994

[127] Baik H.J., Hong S., Park S. Surface plasmon modes of gold nanospheres, nanorods, and nanoplates in an organic solvent: phase-transfer from aqueous to organic media. *J. Colloid Interface Sci.* 2011, **358** pp. 317–322

[128] Yang J., Lee J.Y., Ying J.Y. Phase transfer and its applications in nanotechnology. *Chem. Soc. Rev.* 2011, **40** pp. 1672–1696

[129] Omanovic-Miklicanin E., Valzacchi S., Simoneau C., Gilliland D., Rossi F. Solid-phase microextraction/gas chromatography-mass spectrometry method optimization for characterization of surface adsorption forces of nanoparticles. *Anal. Bioanal. Chem.* 2014, **406** pp. 6629–6636

[130] Wei Z., Sandron S., Townsend A.T., Nesterenko P.N., Paull B. Determination of trace labile copper in environmental waters by magnetic nanoparticle solid phase extraction and high-performance chelation ion chromatography. *Talanta.* 2015, **135** pp. 155–162

[131] Wan Ibrahim W.A., Nodeh H.R., Aboul-Enein H.Y., Sanagi M.M. Magnetic solid-phase extraction based on modified ferum oxides for enrichment, preconcentration, and isolation of pesticides and selected pollutants. *Crit. Rev. Anal. Chem.* 2015, **45** pp. 270–287

[132] Karimi M.A., Hatefi-Mehrjardi A., Mohammadi S.Z., Mohadesi A., Mazloum-Ardakani M., Kabir A.A. Solid phase extraction of trace amounts of silver (I) using dithizone-immobilized alumina-coated magnetite nanoparticles prior to determination by flame atomic absorption spectrometry. *Int. J. Environ. Anal. Chem.* 2012, **92** pp. 1325–1340

[133] Azizi P., Golshekan M., Shariati S., Rahchamani J. Solid phase extraction of Cu2+, Ni2+, and Co^{2+} ions by a new magnetic nano-composite: excellent reactivity combined with facile extraction and determination. *Environ. Monit. Assess.* 2015, **187** p. 185

[134] Chao J.B., Liu J.F., Yu S.J., Feng Y.D., Tan Z.Q., Liu R. Speciation analysis of silver nanoparticles and silver ions in antibacterial products and environmental waters via cloud point extraction-based separation. *Anal. Chem.* 2011, **83** pp. 6875–6882

[135] Hartmann G., Baumgartner T., Schuster M. Influence of particle coating and matrix constituents on the cloud point extraction efficiency of silver nanoparticles (Ag-NPs) and application for monitoring the formation of Ag-NPs from Ag. *Anal. Chem.* 2014, **86** pp. 790–796

[136] Liu J.F., Liu R., Yin Y.G., Jiang G.B. Triton X-114 based cloud point extraction: a thermoreversible approach for separation/concentration and dispersion of nanomaterials in the aqueous phase. *Chem. Commun. (Camb.).* 2009, pp. 1514–1516

[137] Mwilu S.K., Siska E., Baig R.B., Varma R.S., Heithmar E., Rogers K.R. Separation and measurement of silver nanoparticles and silver ions using magnetic particles. *Sci. Total Environ.* 2014, **472** pp. 316–323

[138] Zook J.M., Long S.E., Cleveland D., Geronimo C.L., MacCuspie R.I. Measuring silver nanoparticle dissolution in complex biological and environmental matrices using UV-visible absorbance. *Anal. Bioanal. Chem.* 2011, **401** pp. 1993–2002

[139] Kent R.D., & Vikesland P.J. Controlled evaluation of silver nanoparticle dissolution using atomic force microscopy. *Environ. Sci. Technol.* 2012, **46** pp. 6977–6984

[140] Tulve N.S., Stefaniak A.B., Vance M.E., Rogers K., Mwilu S., LeBouf R.F. Characterization of silver nanoparticles in selected consumer products and its relevance for predicting children's potential exposures. *Int. J. Hyg. Environ. Health.* 2015, **218** pp. 345–357

[141] Taghavy A., Mittelman A., Wang Y., Pennell K.D., Abriola L.M. Mathematical modeling of the transport and dissolution of citrate-stabilized silver nanoparticles in porous media. *Environ. Sci. Technol.* 2013, **47** pp. 8499–8507

[142] Laborda F., Jiménez-Lamana J., Boleaa E., Castillo J.R. Selective identification, characterization and determination of dissolved silver(I) and silver nanoparticles based on single particle detection by inductively coupled plasma-mass spectrometry. *J. Anal. At. Spectrom.* 2011, **26** pp. 1362–1371

[143] Mitrano D.M., Barber A., Bednar A., Westerhoff P., Higginsd C.P., Ranville J.F. Silver nanoparticle characterization using single particle ICP-MS (SP-ICP-MS) and asymmetrical flow field flow fractionation ICP-MS (AF4-ICP-MS). *J. Anal. At. Spectrom.* 2012a, **27** pp. 1131–1142

[144] Mitrano D.M., Lesher E.K., Bednar A., Monserud J., Higgins C.P., Ranville J.F. Detecting nanoparticulate silver using single-particle inductively coupled plasma–mass spectrometry. Environ. Toxicol. Chem. 2012b, **31** pp. 115–121

[145] Reed R.B., Ladner D.A., Higgins C.P., Westerhoff P., Ranville J.F. Solubility of nano-zinc oxide in environmentally and biologically important matrices. *Environ. Toxicol. Chem.* 2012, **31** pp. 93–99

[146] Bednar A.J., Poda A.R., Mitrano D.M., Kennedy A.J., Gray E.P., Ranville J.F. Comparison of on-line detectors for field flow fractionation analysis of nanomaterials. *Talanta.* 2013, **104** pp. 140–148

[147] Mitrano D.M., Ranville J.F., Bednar A.J., Kazor K., Heringd A.S., Higgins C.P. Tracking dissolution of silver nanoparticles at environmentally relevant concentrations in laboratory, natural, and processed waters using single particle ICP-MS (spICP-MS). *Environ. Sci. Nano.* 2014, **1** pp. 248–259

[148] Mercer T.T. On the role of particle size in the dissolution of lung burdens. *Health Phys.* 1967, **13** pp. 1211–1221

[149] Moss O.R., & Kanapilly G.M. 1980) *Dissolution of inhaled aerosols. In: Generation of Aerosols and Facilities for Exposure Experiments* (K. Willeke, Ed.), Ann Arbor Science Publishers Inc., Ann Arbor, MI Publishers, pp. 105-124

[150] Potter R.M., & Mattson S.M. Glass fiber dissolution in a physiological saline solution. Glastech. Ber. 1991, **64** pp. 16–28

[151] Gerischer H., & Sorg N. Chemical dissolution of zinc oxide crystals in aqueous electrolytes - An analysis of the kinetics. *Electrochim. Acta.* 1992, **37** pp. 827–835

[152] Newell C.J., Rifai H.S., Wilson J.T., Connor J.A., Aziz J.A., Suarez M.P. *Calculation and use of first-order rate constants for monitored natural attenuation studies.* United States Environmental Protection Agency, National Risk Management Research Laboratory, 2002

[153] Hume L.A. *The dissolution rate of chrysotile*. Virginia Polytechnic Institute and State University, 1991

[154] Robie R.A., Hemmingway B.S., Fisher J.R. *Thermodynamic properties of minerals and related substances at 298.15 K and 1 bar pressure and at higher temperatures. .*, **Vol. 1452**, 1979, p.

[155] Rimstidt J.D., & Barnes H.L. The kinetics of silica-water reactions. *Geochim. Cosmochim. Acta*. 1980, **44** pp. 1683–1699

[156] Icenhower J., & Dove P. The dissolution kinetics of amorphous silica into sodium chloride solutions: Effects of temperature and ionic strength. *Geochim. Cosmochim. Acta*. 2000, **64** pp. 4193–4203

[157] Rosso J.J., & Rimstidt J.D. A high resolution study of forsterite dissolution rates. *Geochim. Cosmochim. Acta*. 2000, **64** pp. 797–811

[158] Jurinski J.B., & Rimstidt J.D. Biodurability of talc. *Am. Mineral.* 2001, **86** pp. 392–399

[159] Roelofs F., & Vogelsberger W. Dissolution kinetics of synthetic amorphous silica in biological-like media and its theoretical description. *J. Phys. Chem. B.* 2004, **108** pp. 11308–11316

[160] Schmidt J., & Vogelsberger W. Aqueous Long-Term Solubility of Titania Nanoparticles and Titanium(IV) Hydrolysis in a Sodium Chloride System Studied by Adsorptive Stripping Voltammetry. *J. Solution Chem.* 2009, **38** pp. 1267–1282

[161] Larson R.R., Story S.G., Hegmann K.T. Assessing the Solubility of Silicon Dioxide Particles Using Simulated Lung Fluid. *Open Toxic J.* 2010, **4** pp. 51–55

[162] Huang W., Fernandez D., Rudd A., Johnson W.P., Deubner D., Sabey P. Dissolution and nanoparticle generation behavior of Be-associated materials in synthetic lung fluid using inductively coupled plasma-mass spectroscopy and flow field-flow fractionation. *J. Chromatogr. A.* 2011, **1218** pp. 4149–4159

[163] Duling M.G., Stefaniak A.B., Lawrence R.B., Chipera S.J., Virji M.A. Release of beryllium from mineral ores in artificial lung and skin surface fluids. *Environ. Geochem. Health.* 2012, **34** pp. 313–322

[164] Finch G.L., Mewhinney J.A., Eidson A.F., Hoover M.D., Rothenberg S.J. In vitro dissolution characteristics of beryllium oxide and beryllium metal aerosols. *J. Aerosol Sci.* 1988, **19** pp. 333–342

[165] Stefaniak A.B., Day G.A., Hoover M.D., Breysse P.N., Scripsick R.C. Differences in dissolution behavior in a phagolysosomal simulant fluid for single-constituent and multi-constituent materials associated with beryllium sensitization and chronic beryllium disease. *Toxicol. In Vitro.* 2006, **20** pp. 82–95

[166] Stefaniak A.B., Virji M.A., Day G.A. Dissolution of beryllium in artificial lung alveolar macrophage phagolysosomal fluid. *Chemosphere.* 2011, **83** pp. 1181–1187

[167] Stefaniak A.B., Virji M.A., Day G.A. Release of beryllium into artificial airway epithelial lining fluid. *Arch. Environ. Occup. Health.* 2012, **67** pp. 219–228

[168] Liu X., Hurt R.H., Kane A.B. Biodurability of Single-Walled Carbon Nanotubes Depends on Surface Functionalization. *Carbon N Y.* 2010, **48** pp. 1961–1969

[169] Kagan V.E., Konduru N.V., Feng W., Allen B.L., Conroy J., Volkov Y. Carbon nanotubes degraded by neutrophil myeloperoxidase induce less pulmonary inflammation. *Nat. Nanotechnol.* 2010, **5** pp. 354–359

[170] Osmond-McLeod M.J., Poland C.A., Murphy F., Waddington L., Morris H., Hawkins S.C. Durability and inflammogenic impact of carbon nanotubes compared with asbestos fibres. *Part. Fibre Toxicol.* 2011, **8** p. 15

[171] ZHAO Y., ALLEN B.L., STAR A. Enzymatic degradation of multiwalled carbon nanotubes. *J. Phys. Chem. A*. 2011, **115** pp. 9536–9544

[172] LEE Y.J., KIM J., OH J., BAE S., LEE S., HONG I.S. Ion-release kinetics and ecotoxicity effects of silver nanoparticles. *Environ. Toxicol. Chem.* 2012, **31** pp. 155–159

[173] MA R., LEVARD C., MARINAKOS S.M., CHENG Y., LIU J., MICHEL F.M. Size-Controlled Dissolution of Organic-Coated Silver Nanoparticles. *Environ. Sci. Technol.* 2012, **46** pp. 752–759

[174] LEVARD C., MITRA S., YANG T., JEW A.D., BADIREDDY A.R., LOWRY G.V. Effect of Chloride on the Dissolution Rate of Silver Nanoparticles and Toxicity to E. coli. *Environ. Sci. Technol.* 2013, **47** pp. 5738–5745

[175] GORHAM J.M., MACCUSPIE R.I., KLEIN K.L., FAIRBROTHER D.H., HOLBROOK R.D. UV-induced photochemical transformations of citrate-capped silver nanoparticle suspensions. *J. Nanopart. Res.* 2012, **14** pp. 1–16

[176] YIN Y., LIU J., JIANG G. Sunlight-induced reduction of ionic Ag and Au to metallic nanoparticles by dissolved organic matter. *ACS Nano*. 2012, **6** pp. 7910–7919

[177] BEHRA R., SIGG L., CLIFT M.J., HERZOG F., MINGHETTI M., JOHNSTON B. Bioavailability of silver nanoparticles and ions: from a chemical and biochemical perspective. *J. R. Soc. Interface.* 2013, **10** p. 20130396

[178] LEE J.H., KIM Y.S., SONG K.S., RYU H.R., SUNG J.H., PARK J.D. Biopersistence of silver nanoparticles in tissues from Sprague-Dawley rats. *Part. Fibre Toxicol.* 2013, **10** p. 36

[179] KHAN F.R., MISRA S.K., GARCÍA-ALONSO J., SMITH B.D., STREKOPYTOV S., RAINBOW P.S. Bioaccumulation dynamics and modeling in an estuarine invertebrate following aqueous exposure to nanosized and dissolved silver. *Environ. Sci. Technol.* 2012, **46** pp. 7621–7628

[180] STEBOUNOVA L.V., GUIO E., GRASSIAN V.H. Silver nanoparticles in simulated biological media: a study of aggregation, sedimentation, and dissolution. *J. Nanopart. Res.* 2011, **13** pp. 233–244

[181] SCHMIDT J., & VOGELSBERGER W. Dissolution Kinetics of Titanium Dioxide Nanoparticles: The Observation of an Unusual Kinetic Size Effect. *J. Phys. Chem. B.* 2006, **110** pp. 3955–3963

[182] HEDBERG Y., HEDBERG J., WALLINDER I.O. Particle Characteristics and Metal Release from Natural Rutile (TiO$_2$) and Zircon Particles in Synthetic Body Fluids. *J Biomaterials Nanobio*. 2012, **3** pp. 37–49

[183] AVRAMESCU M.L., RASMUSSEN P.E., CHENIER M., GARDNER H.D. Influence of pH, particle size and crystal form on dissolution behaviour of engineered nanomaterials. *Environ. Sci. Pollut. Res. Int.* 2016, ••• pp. 1–12

[184] BIAN S.W., MUDUNKOTUWA I.A., RUPASINGHE T., GRASSIAN V.H. Aggregation and dissolution of 4 nm ZnO nanoparticles in aqueous environments: influence of pH, ionic strength, size, and adsorption of humic acid. *Langmuir.* 2011, **27** pp. 6059–6068

[185] YANG S.-T., WANG H., MEZIANI M.J., LIU Y., WANG X., SUN Y.-P. Biodefunctionalization of Functionalized Single-Walled Carbon Nanotubes in Mice. *Biomacromolecules.* 2009, **10** pp. 2009–2012

[186] CHANANA M., GIL P.R., CORREA-DUARTE M.A., LIZ-MARZAN L.M., PARAK W.J. Physicochemical Properties of Protein-Coated Gold Nanoparticles in Biological Fluids and Cells before and after Proteolytic Digestion. *J. Angew. Chem. Int. Ed.* 2013, **52** pp. 4179–4183

[187] ROBERTS A.P., MOUNT A.S., SEDA B., SOUTHER J., QIAO R., LIN S. *In vivo* Biomodification of Lipid-Coated Carbon Nanotubes by *Daphnia magna. Environ. Sci. Technol.* 2007, **41** pp. 3025–3029

[188] ULBRICHT J., JORDAN R., LUXENHOFER R. On the biodegradability of polyethylene glycol, polypeptoids and poly(2-oxazoline)s. *Biomaterials.* 2014, **35** pp. 4848–4861

[189] Marvin L.F., Roberts M.A., Fay L.B. Matrix-assisted laser desorption/ionization time-of-flight mass spectrometry in clinical chemistry. *Clin. Chim. Acta.* 2003, **337** pp. 11–21

[190] Yan B., Jeong Y., Mercante L.A., Tonga G.Y., Kim C., Zhu Z.J. Characterization of surface ligands on functionalized magnetic nanoparticles using laser desorption/ionization mass spectrometry (LDI-MS). *Nanoscale.* 2013a, **5** pp. 5063–5066

[191] Yan B., Kim S.T., Kim C.S., Saha K., Moyano D.F., Xing Y. Multiplexed imaging of nanoparticles in tissues using laser desorption/ionization mass spectrometry. *J. Am. Chem. Soc.* 2013b, **135** pp. 12564–12567

[192] Zhu Z.J., Yeh Y.C., Tang R., Yan B., Tamayo J., Vachet R.W. Stability of quantum dots in live cells. *Nat. Chem.* 2011, **3** pp. 963–968

[193] Zhu Z.J., Tang R., Yeh Y.C., Miranda O.R., Rotello V.M., Vachet R.W. Determination of the intracellular stability of gold nanoparticle monolayers using mass spectrometry. *Anal. Chem.* 2012, **84** pp. 4321–4326

[194] Harder P., Grunze M., Dahint R., Whitesides G.M., Laibinis P.E. Molecular Conformation in Oligo(ethylene glycol)-Terminated Self-Assembled Monolayers on Gold and Silver Surfaces Determines Their Ability To Resist Protein Adsorption. *J. Phys. Chem. B.* 1998, **102** pp. 426–436

[195] Valiokas R., Svedhem S., Svensson S.C.T., Liedberg B. Selfassembled, monolayers of oligo(ethylene glycol)-terminated and amide group containing alkanethiolates on gold. *Langmuir.* 1999, **15** pp. 3390–3394

[196] Valiokas R., Svedhem S., Ostblom M., Svensson S.C.T., Liedberg B. Influence of specific intermolecular interactions on the self-assembly and phase behavior of oligo(ethylene glycol)-terminated alkanethiolates on gold. *J. Phys. Chem. B.* 2001, **105** pp. 5459–5469

[197] Monopoli M.P., Walczyk D., Campbell A., Elia G., Lynch I., Bombelli F.B. Physical-chemical aspects of protein corona: relevance to in vitro and in vivo biological impacts of nanoparticles. *J. Am. Chem. Soc.* 2011, **133** pp. 2525–2534

[198] Mahmoudi M., Lohse S.E., Murphy C.J., Fathizadeh A., Montazeri A., Suslick K.S. Variation of protein corona composition of gold nanoparticles following plasmonic heating. *Nano Lett.* 2014, **14** pp. 6–12

[199] Ansoborlo E., Chalabreysse J., Escallon S., Henge-Napoli M.H. *In vitro* solubility of uranium tetrafluoride with oxidizing medium compared with in vivo solubility in rats. *Int. J. Radiat. Biol.* 1990, **58** pp. 681–689

[200] Julander A., Hindsen M., Skare L., Liden C. Cobalt-containing alloys and their ability to release cobalt and cause dermatitis. *Contact Dermat.* 2009, **60** pp. 165–170

[201] Day G.A., Hoover M.D., Stefaniak A.B., Dickerson R.M., Peterson E.J., Esmen N.A. Bioavailability of beryllium oxide particles: an in vitro study in the murine J774A.1 macrophage cell line model. *Exp. Lung Res.* 2005, **31** pp. 341–360

[202] Finch G.L., Mewhinney J.A., Hoover M.D., Eidson A.F., Haley P.J., Bice D.E. Clearance, translocation, and excretion of beryllium following acute inhalation of beryllium oxide by beagle dogs. *Fundam. Appl. Toxicol.* 1990, **15** pp. 231–241

[203] Jeong J., Kim J., Seok S.H., Cho W.S. Indium oxide (InO) nanoparticles induce progressive lung injury distinct from lung injuries by copper oxide (CuO) and nickel oxide (NiO) nanoparticles. *Arch. Toxicol.* 2015

[204] Borm P., Klaessig F.C., Landry T.D., Moudgil B., Pauluhn J., Thomas K. Research strategies for safety evaluation of nanomaterials, part V: role of dissolution in biological fate and effects of nanoscale particles. *Toxicol. Sci.* 2006, **90** pp. 23–32

[205] Schroeter J.D., Nong A., Yoon M., Taylor M.D., Dorman D.C., Andersen M.E. Analysis of manganese tracer kinetics and target tissue dosimetry in monkeys and humans with multi-route physiologically-based pharmacokinetic models. *Toxicol. Sci.* 2011, **120** pp. 481–498

[206] Schroeter J.D., Dorman D.C., Yoon M., Nong A., Taylor M.D., Andersen M.E. Application of a multi-route physiologically-based pharmacokinetic model for manganese to evaluate dose-dependent neurological effects in monkeys. *Toxicol. Sci.* 2012, **129** pp. 432–446

[207] Taylor M.D., Clewell H.J., Andersen M.E., Schroeter J.D., Yoon M., Keene A.M. Update on a Pharmacokinetic-Centric Alternative Tier II Program for MMT-Part II: Physiologically-Based Pharmacokinetic Modeling and Manganese Risk Assessment. *J. Toxicol.* 2012, **2012** p. 791431

[208] Canady R.A. The uncertainty of nanotoxicology: report of a Society for Risk Analysis Workshop. *Risk Anal.* 2010, **30** pp. 1663–1670

[209] Som C., Berges M., Chaudhry Q., Dusinska M., Fernandes T.F., Olsen S.I. The importance of life cycle concepts for the development of safe nanoproducts. *Toxicology.* 2010, **269** pp. 160–169

[210] Donaldson K., Murphy F., Schinwald A., Duffin R., Poland C.A. Identifying the pulmonary hazard of high aspect ratio nanoparticles to enable their safety-by-design. *Nanomedicine (Lond.).* 2011, **6** pp. 143–156

[211] Batley G.E., Halliburton B., Kirby J.K., Doolette C.L., Navarro D., McLaughlin M.J. Characterization and ecological risk assessment of nanoparticulate CeO2 as a diesel fuel catalyst. *Environ. Toxicol. Chem.* 2013, **32** pp. 1896–1905

[212] Thelohan S., & de Meringo A. *In vitro* dynamic solubility test: influence of various parameters. *Environ. Health Perspect.* 1994, **102** () pp. 91–96

[213] Takaya M., Shinohara Y., Serita F., Ono-Ogasawara M., Otaki N., Toya T. Dissolution of functional materials and rare earth oxides into pseudo alveolar fluid. *Ind. Health.* 2006, **44** pp. 639–644

[214] EPA. 1993) Methods for measuring the acute toxicity of effluents and receiving waters to freshwater and marine organisms, fourth edition. edit: Cornilius L. Weber. EPA/600/4-90/027F. Section 7: Dilution Water, page 30

[215] Marking L.L., & Dawson V.K. *Toxicity of quinaldine sulfate to fish. Invest. Fish Contr.* US Fish and Wildlife Service, Department of the Interior, Washington, D. C., 1973, p.

[216] IOC. *Standard and Reference Materials for Marine Science. Intergovernmental Oceanographic Commission. Manuals and Guides.* UNESCO, 1990

[217] ISO/TS 27687:2008, *Nanotechnologies — Terminology and definitions for nano-objects — Nanoparticle, nanofibre and nanoplate*

Amendments Issued Since Publication

Amend No.	Date of Issue	Text Affected